Chapter 9

Long-term projections of stratospheric ozone

Lead authors: John Austin & John Scinocca

Co-authors: Trevor Bailey
Luke Oman
David Plummer
David Stephenson
Hamish Struthers

9.1 Introduction

The long-term evolution of ozone is influenced by a wide variety of factors that may be broadly separated into radiative, dynamical, transport, chemical and external forcing processes. Many of the processes are also coupled in the sense that, for example, dynamical changes lead to chemical changes, which feed back onto the dynamics. Therefore, although it is convenient to try to separate the effects of individual processes on ozone amounts, to some extent this can be a matter of definition and the stratosphere needs to be treated as a whole.

Radiative effects related to ozone were discussed in Chapter 3. Stratospheric temperature (and hence ozone chemistry) is influenced by radiative processes through changes in the long-lived greenhouse gases (GHGs) (Shine *et al*., 2003); primarily CO_2, although CH_4, H_2O, and N_2O are minor contributors. The stratospheric temperature also has an important influence on the formation of polar stratospheric clouds, which are implicated in polar ozone destruction. Ozone itself is a radiative gas. The radiative effects combined — due to GHGs and ozone — induce temperature changes. In turn this changes the planetary wave driving of the Brewer-Dobson (BD) circulation, which on climate time scales leads to increased transport (Butchart and Scaife, 2001).

Dynamical effects related to ozone were discussed in Chapter 4. Ozone amounts are influenced by both resolved and parameterised wave forcing. Resolved waves include synoptic scale and planetary waves, which have in particular a direct effect on the polar vortex. Most models include parameterisations for both orographic and non-orographic gravity waves (Chapter 2), which are crucial to simulate realistic polar vortex strength. For those models that have sufficient vertical resolution, there is the potential to model a spontaneous Quasi-Biennial Oscillation (QBO) (Takahashi, 1996). The QBO is an important part of the tropical variability, but also contributes to interannual variability in high latitude stratospheric winds by the well-known Holton-Tan effect (Holton and Tan, 1980). These processes have a direct effect on ozone amounts through transport. Dynamical processes also influence temperatures which in turn affect the chemistry of ozone because of the temperature dependence of the reaction rates.

Transport effects were discussed in Chapter 5. The net ozone change is essentially the balance between transport and chemistry, and small changes such as those due to the changes in the BD circulation (Shepherd, 2008) can have important direct changes on ozone as well as influencing the concentrations of long-lived species, in particular Cl_y and NO_y, which produce further chemical changes (Douglass *et al*., 2008).

Chemical effects related to ozone were discussed in Chapter 6. Chemical processes in recent decades have been dominated by the evolution of halogen loading (Eyring *et al*., 2006), which will also remain the focus of attention for several decades to come. While chlorine remains present in high concentrations in the atmosphere, volcanic eruptions will also play an important role through the supply of sites for heterogeneous reactions (Tie and Brasseur, 1995). Changes in water vapour concentration have a dual role; in changing the concentration of HO_x radicals, and in changing the amount of polar stratospheric clouds (PSCs). HO_x catalytically destroys ozone and changes the balance of other chemical species. Increases in PSC amounts lead to enhanced ozone destruction in the presence of high halogen amounts. N_2O increases lead to increased NO_y, and future ozone loss (Portmann and Solomon, 2007).

The UTLS region (Chapter 7) is important to ozone since, for example, water vapour concentrations in the stratosphere depend on the tropical tropopause temperature. The tropical pipe (Plumb, 1996) is also a source of very short-lived species which contribute to ozone depletion (WMO, 2007, Chapter 2).

Forcings external to the atmosphere also contribute to ozone change and were discussed in Chapter 8. At the top of the atmosphere, solar cycle variability leads to changes in ultraviolet (UV) flux which contributes to ozone variability *via* changes in photolysis rates (Austin *et al*., 2008). Unlike most other processes considered, though, this is cyclic rather than systematic, apart from historical periods such as the Maunder Minimum of several centuries ago. The lower boundary of the atmosphere is coupled to the sea surface, which will influence and be influenced by tropospheric dynamics, which in turn can affect stratospheric wave propagation (Garnkel and Hartman, 2007). Volcanic aerosols also affect ozone through heterogeneous chemical effects and *via* radiative heating (Chapter 3). Finally, the extent to which sea-surface temperatures (SSTs) and the troposphere influence the stratosphere will be determined in small part by the effect of the stratosphere on climate (Chapter 10).

The degree to which all of these factors combined influence the future evolution of ozone is investigated using the simulations of CCMVal-2, described in Chapter 2. The two sets of results from experiments REF-B1 and REF-B2 are used. In REF-B1, sea surface temperatures (SSTs) and external forcing parameters including the solar cycle, were specified from observations. In REF-B2, the greenhouse gas (GHG) scenario SRES A1b and the halogen scenario A1 from WMO (2007) were used to investigate the future behaviour of stratospheric ozone until the end of the 21st century. The results are found to depend broadly on latitude and hence it is most natural to divide the results into tropical, mid-latitude, and polar regions. For each of these regions the goal of this Chapter will be:

- To review and update our understanding of the dominant factors that affect ozone depletion and recovery in that region.
- To present the projected past and future ozone change from the new (CCMVal-2) CCM simulations and compare this with the projected ozone change from the previous (CCMVal-1) CCM simulations.
- To pull together "future-change" information for these factors from the relevant chapters of this report to understand the evolution of ozone and to estimate the relative importance of any competing factors.
- To identify outstanding modelling issues that are central to the accurate prediction of long-term ozone in that region.

In addition, in Section 9.6 the results from the different regions are brought together to address the issue of ozone recovery and its timing. The 2006 Ozone assessment (WMO, 2007) expressed ozone recovery in terms of ozone increase relating to a reduction in ozone depleting substances (ODSs). Here, we need to consider a more generalised ozone recovery, which takes account of changes in GHGs as well. In this respect ozone recovery can be considered in the same way as tropospheric temperature change, and attribution analyses can be undertaken to determine the cause of ozone recovery, whether it is chemical (*via* ODS reduction for example), radiative (*via* temperature change on the reaction rates) or dynamical (*via* chang-

es in transport). Hence, we use the term "ozone recovery" to imply the process of an increase in ozone. We avoid terms such as "full recovery" and "super-recovery", which imply the need for an ozone or ODS benchmark. Instead, we refer to points along the path of ozone increase as "recovery to 1980 levels" or "return to 1980 levels". We also consider other reference dates, such as 1960, reflecting the loss of ozone that likely occurred prior to the availability of extensive satellite measurements of ozone.

9.2 Analysis methods

The CCMVal results are investigated using two distinct analysis methods. In Section 9.2.1 we present a multi-model time series analysis method which is used to document the evolution of total column ozone and chlorine amounts. In Section 9.2.2 we summarize the multi-linear regression methodology that is used to attribute individual model sensitivities to chemistry and temperature.

9.2.1 Multi-Model Time Series Analysis

Ideally, a comparison between CCMVal-1 and CCMVal-2 projections would be based on analyses that produced quantitative predictions and uncertainty estimates of ozone and ozone related indices. In previous studies, time series analysis of CCMVal simulations (WMO 2007, Eyring *et al*., 2007) have provided mostly qualitative results making it difficult to formulate and utilize multi-model projections. Instead, we formulate a new analysis procedure based on a statistical framework that employs a nonparametric additive model to estimate individual-model trends (IMT) and multi-model, trends (MMT). Here, the term "trend" refers to a smooth trajectory passing through the time series data representing the "signal", leaving a "noise" field as the residual. The goal in this procedure is the definition of the simplest nonparametric additive model whose trend estimate produces residuals that satisfy assumed properties of noise (*e.g*., that it be an independent normally distributed random variable). The use of a statistical framework based on a probabilistic model allows the trend estimates to be used to make formal inference (*e.g*., calculation of confidence and prediction intervals). We shall refer to this new time series additive-model analysis as the "TSAM" analysis. Attractive properties of the TSAM analysis include: the production of smooth trend estimates out to the ends of the time series, the ability to model explicitly interannual variability about the trend estimate, and the ability to make rigorous probability statements. Because the TSAM analysis is based on a testable probabilistic model, the suitability of the particular nonparametric additive model used can be validated.

The TSAM analysis adopted here consists of three steps: estimation of individual model trends (IMT), baseline adjustment of these trends, and the weighted combination of the IMT estimates to produce a multi-model trend (MMT) estimate. Much of the development effort of the TSAM analysis has gone into the final weighting step. The formulation allows the specication of prior model weights if this is desired (*e.g*., metric-based performance weighting, although in the present application of the TSAM, this feature was not used) in the evaluation of the final MMT estimate. Two types of uncertainty intervals are constructed for the MMT estimate. The first is the point-wise 95% confidence interval. This interval has a 95% chance of overlapping the true trend, representing the local uncertainty in the trend at each year. The second interval, larger by construction, is the 95% prediction interval. This interval is a combination of uncertainty in the trend estimate and uncertainty due to natural interannual variability about the trend. It gives an idea of where an ozone value for a given year might reasonably lie.

A complete description of the TSAM is provided in Appendix B. along with detailed examples of its application. A supplement to the chapter has been created in which a more complete set of TSAM diagnostics are provided along with an analysis of its sensitivity to outliers and a comparison with the simpler methods of time series analysis employed for CCMVal-1.

In the following sections, three types of figures will be presented that relate to the application of the TSAM analysis on ozone related time series. The first (*e.g*., Figure 9.1 left-hand column) represents initial IMT estimates of the raw time series data. This initial smooth fit is used to define a baseline value for each model, and a multi-model mean baseline value for a specified reference year. Taking the reference year as 1980 for example, anomaly time series would be constructed by taking the raw time series and subtracting their respective 1980 baseline values. Finally, to each anomaly time series the multi-model mean 1980 baseline value would be added. In this example, we would refer to these as "1980 baseline-adjusted" time series. The second type of figure (*e.g*., Figure 9.1 right-hand column) displays IMT estimates of the baseline-adjusted time series and it is these that are used to define the MMT estimate in the final step of the TSAM analysis. The third type of figure (*e.g*., Figure 9.2) shows the baseline-adjusted MMT estimate (heavy dark-grey line) along with its 95% confidence, and 95% prediction intervals (light- and dark-grey shading respectively). Further details may be found in Appendix B and a complete set of these figures appears in Section 9S.1 of the supplement to this chapter. The final MMT estimates are suitable for the production of multi-model estimates of return dates and this is discussed in Section 9.6.

9.2.2 Multi-linear regression analysis

Multiple linear regression (MLR) is used to deter-

mine the relationship between ozone amounts and physical parameters to try to obtain the reasons for the modelled ozone trends. We concentrate on the middle and upper stratosphere, where the processes are more amenable to this analysis. The method used here is based on Oman *et al*. (2010) which separates the contributions of explanatory variables to changes in extra-polar ozone. As discussed in Oman *et al*. (2010), the MLR method focuses on the variables contributing to ozone change rather than the specific surface forcings (*e.g*., CO_2, N_2O, CH_4, and Halogens). The explanatory variables are temperature, NO_y, HO_x and $Cl_y + \alpha Br_y$. For those models which did not supply HO_x (AMTRAC3 and UMUKCA-UCAM) this term was not included in the analysis. Likewise, several models (CAM3.5, CNRM-ACM, UMSLIMCAT, and UMUKCA-UCAM) did not supply bromine, or bromine was not included in the simulations, and so the bromine component of $Cl_y + \alpha Br_y$ was set to zero.

The purpose of the analysis is to estimate the contribution of the different chemical mechanisms to the simulated changes in ozone. The principal analysis method used is multiple linear regression (MLR), which for a given location is applied to determine the coefficients m_x such that

$$\Delta O_3(t) = \Sigma_j m_{x_j} \Delta x_j(t) + \varepsilon(t) \qquad (9.1)$$

where the x_j are the independent parameters of the regression and $\varepsilon(t)$ is the residual. Four explanatory variables x_j are used: $Cl_y + \alpha Br_y$, $NO_y = NO + NO_2 + NO_3 + 2N_2O_5 + HNO_3 + HNO_4 + ClONO_2 + BrONO_2$, $HO_x = OH + HO_2$, and temperature, T. m_{x_j} is later referred to as the 'sensitivity' of O_3 to the independent parameter x_j. Each of the product terms on the right hand side of Equation 9.1, $m_{x_j} \Delta x_j(t)$, represents the contribution of x_j to the ozone change. For the term $Cl_y + \alpha Br_y$, α is taken to be 5, the appropriate value for the upper stratosphere (Daniel *et al*., 1999), which is the region of the atmosphere considered here.

The MLR analysis is more difficult to interpret in the lower stratosphere, where photochemical time scales are comparable to the dynamical time scales. Hence temperature changes can induce chemical changes in ozone as well as reflecting dynamical variations which induce transport changes in ozone. Since these effects are often opposed, the resulting regression fit is poorer.

9.3 Tropical Ozone

9.3.1 From the 2006 WMO assessment:

- A small (2%) increase in column ozone is expected from 2000 to 2020.
- The 2050 column ozone is expected to be slightly lower than 1980 values.
- Decreased ozone occurs in the lower stratosphere, due to the enhancement of the BD circulation, which is expected to bring up ozone-poor air from the troposphere.

9.3.2 Further analysis of the CCMVal-1 runs

The strength of the BD circulation is expected to increase on climate time scales (Butchart and Scaife, 2001; Butchart *et al*., 2006; McLandress and Shepherd, 2009a), driven by increases in GHGs. Li *et al*. (2008) and Oman *et al*. (2009) show that the BD circulation is also driven in part by changes in ozone, with the circulation changing fastest during the last two decades when ozone depletion was strongest. In the future, as ozone recovers, the BD circulation is expected to increase less rapidly (Li *et al*., 2008; Oman *et al*., 2009). Model simulations agree well with calculations of upwelling derived from radiosonde observations (Yang *et al*., 2008), although it is not currently feasible to determine observed trends because of the quality of the data. An indirect way of estimating the trend in upwelling is *via* the age of air, which should decrease due to climate change (*e.g*., Austin and Li, 2006; Garcia *et al*., 2007). However, although measurements do not show a trend in age of air (Engel *et al*., 2009), because of their large uncertainties, they do not necessarily contradict CCM results (Waugh, 2009).

The change in the BD circulation gives rise to upward transport of ozone and other constituents in tropical regions, leading to lower tropical ozone in particular (*e.g*., Shepherd, 2008). The decrease of column ozone due to transport is comparable to the increase in the upper stratosphere due to stratospheric temperature change (*e.g*., Li *et al*., 2009).

Recent work has also investigated trends in the position of the tropopause (Son *et al*., 2008; Gettelman *et al*., 2009; Austin and Reichler, 2008). These studies show that the tropopause height is expected to increase in the future at a similar rate as the increase of the past few decades. The tropopause pressure is also simulated to decrease at a similar rate in the future as in the past. Austin and Reichler (2008) also show that in AMTRAC, the BD circulation is closely related to tropopause pressure and that their model simulates larger tropopause pressure trends than observed. These studies combined indicate that models with larger trends in upwelling give rise to larger trends in tropopause pressure, and that the mean of the models considered by Son *et al*. (2008), which included both small BD trends as well as large trends, is in good agreement with observations. In independent calculations, Fomichev *et al*. (2007) also show that an increase in SSTs leads to a warmer and higher tropopause. A plausible physical mechanism for the tropical SST influence is the strengthening of tropical upwelling *via* deep convection (Deckert and Dameris, 2008).

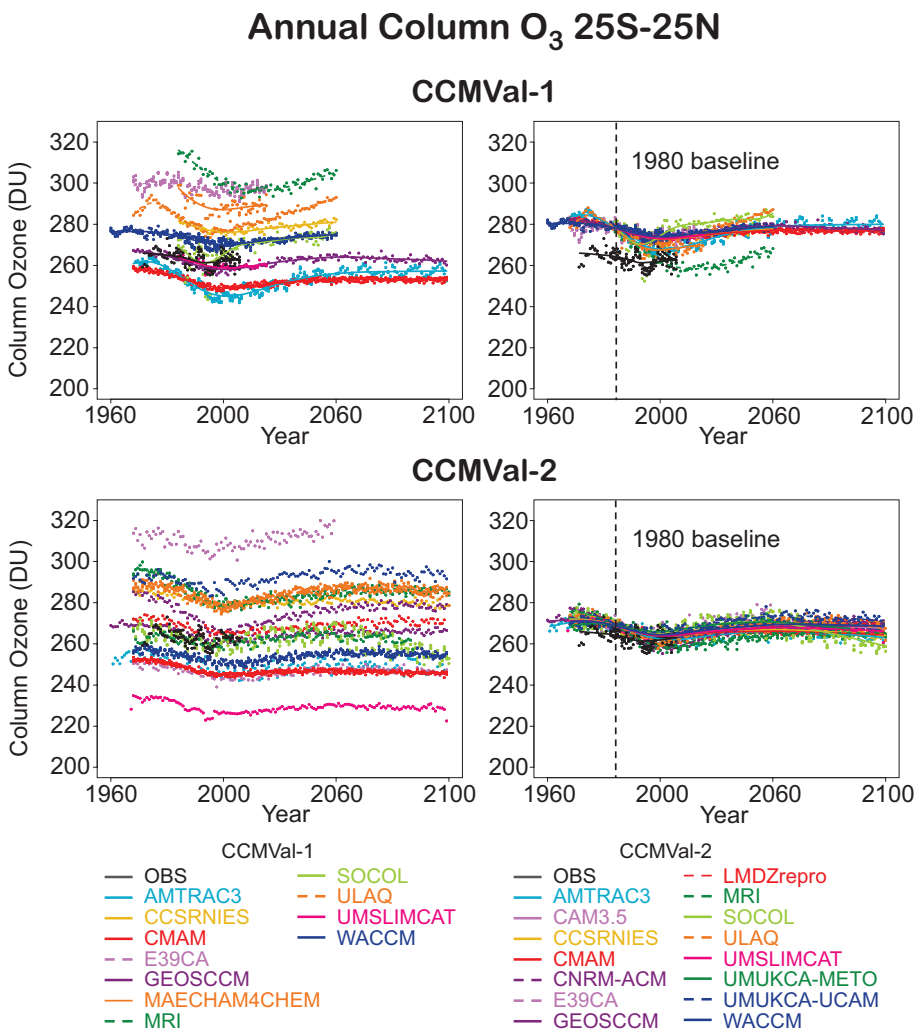

Figure 9.1: Raw time series data of annually averaged total ozone for the latitude range 25°S-25°N and initial individual model trend (IMT) estimates (left-hand panels), and 1980 baseline-adjusted time series data and 1980 baseline-adjusted IMT estimates (right-hand panels) for the TSAM analysis of CCMVal-1 (top) and CCMVal-2 (bottom). Observations are shown in black for four observational data sets (see text). A lowess fit (with smoother span f=0.4) to the observations appears as a black line in all panels. The observations are not baseline-adjusted in the right-hand panels.

The implication of the trend in tropopause pressure is to reduce ozone at a given pressure just above the tropical tropopause. This would also follow directly from the increased upwelling in that region. A reduction in ozone has been observed in that part of the atmosphere (Randel and Wu, 2007) exceeding 6%/decade since 1980, which is too large to be understood on the basis of known chemistry, as radical concentrations are considered too small to have had a significant impact. The trend in ozone in this region has an important radiative impact, which leads to temperature trends in the tropopause region that are in much better agreement with observations than the simulations of the Coupled Model Intercomparison Project 3 (Forster *et al.*, 2007). The advantage of a CCM is that ozone is reasonably accurate in the vicinity of the tropopause, whereas in models with specified ozone, the connection between the local tropopause and the ozone amount is lost, and this has a significant impact on net heating rates (Forster *et al.*, 2007).

9.3.3 Tropical TSAM analysis

The TSAM analysis is applied to both the CCMVal-1 and current CCMVal-2 tropical total column ozone and 50 hPa total inorganic chlorine to identify any changes or improvements in moving to the newer models. In the left-hand column of **Figure 9.1** we present the raw time series data and the initial TSAM individual-model-trend (IMT) estimates for the annual total column ozone in the latitude band 25°S-25°N for 11 CCMVal-1 models (top) and 15 CCMVal-2 models (bottom). These initial IMT estimates

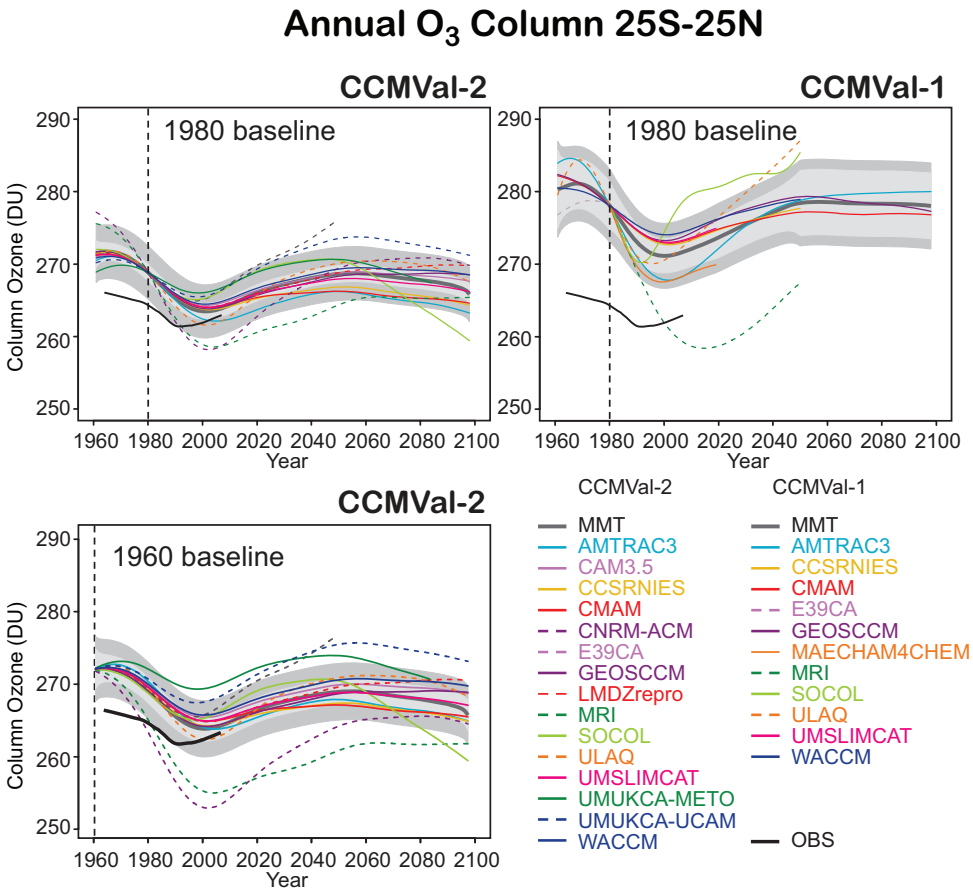

Figure 9.2: 1980 baseline-adjusted multi-model trend (MMT) estimates of annually averaged total ozone for the latitude range 25°S-25°N (heavy dark grey line) with 95% confidence and 95% prediction intervals appearing as light- and dark-grey shaded regions about the trend (upper panels). The baseline-adjusted IMT estimates, and unadjusted lowess fit to the observations are additionally plotted. CCMVal-2 results appear on the left and CCMVal-1 results appear on the right. The lower panel shows the same analysis of CCMVal-2 data but for a baseline adjustment employing a 1960 reference date.

employ the nonparametric additive model discussed in Appendix B and were verified by an analysis of the residuals (*e.g.*, see Appendix B.3). Observations of total ozone from four data sets are also presented in Figure 9.1 (black lines and symbols). These include ground-based measurements (updated from Fioletov *et al.* (2002)), merged satellite data (Stolarski and Frith, 2006), the National Institute of Water and Atmospheric Research (NIWA) combined total column ozone database (Bodeker *et al.*, 2005), and from Solar Backscatter Ultraviolet (SBUV, SBUV/2) retrievals (updated from Miller *et al.* (2002)).

Both the CCMVal-1 and CCMVal-2 time series display a wide range of background total ozone values over the entire REF-B2 period, which extend significantly above and below the observed values in this region. While the biases of most models have remained unchanged between the two inter-comparison projects, two models show significant differences from CCMVal-1 to CCMVal-2: WACCM has changed from a positive bias to a negative bias and UMSLIMCAT has changed from a near zero bias to a signicant negative bias.

As described in Sections 9.2.1 and Appendix B, relative to a selected reference date, baseline-adjusted time series and IMT estimates are computed in the second step of the TSAM analysis to facilitate a closer comparison of the predicted evolution of ozone indices between models. Analogous to the analysis performed in Chapter 6 of WMO (2007) and Eyring *et al.* (2007), anomaly time series are created for each model about a baseline value prior to significant ozone loss. Here, the baseline value is taken to be the initial IMT estimate at a selected reference date for each model (*e.g.*, 1980).

The baseline-adjusted time series are then formed by adding a constant so that each anomaly time series goes through the multi-model average of the IMT estimates at the reference date. Since the multi-model average of the IMT estimates is a close approximation to the final multi-model trend (MMT) estimate derived in the third step

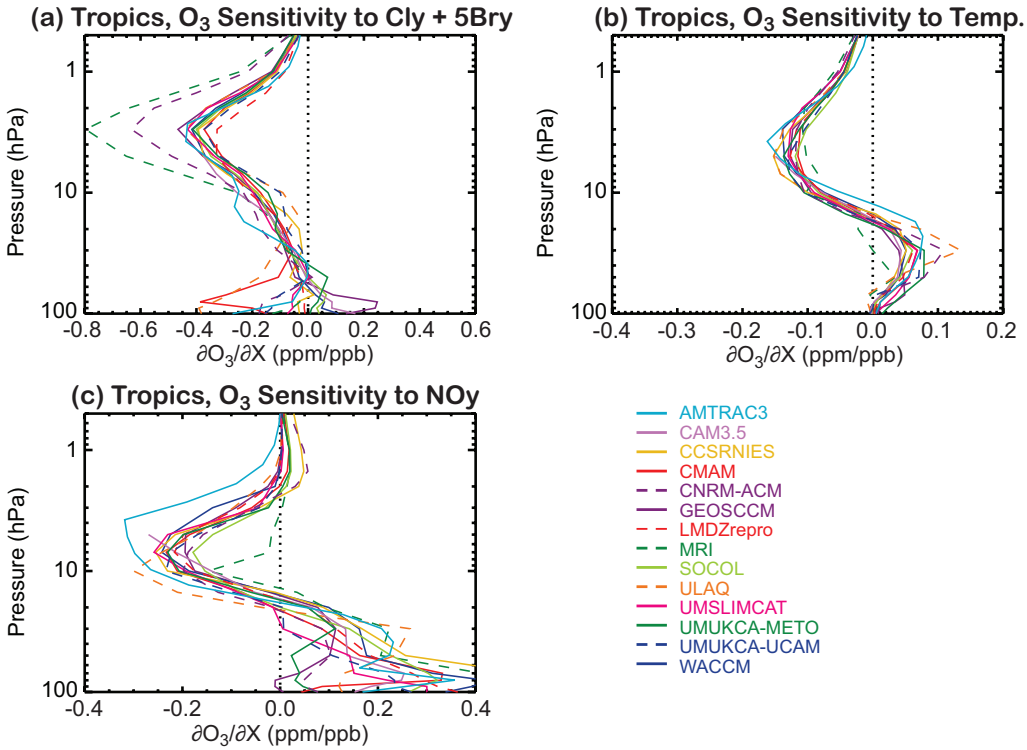

Figure 9.3: Results of the MLR analysis for the CCMVal-2 models in the latitude band 25°S-25°N. (a) Sensitivity of the model ozone to halogen, (b) sensitivity of the model ozone amounts to temperature and (c) sensitivity of the model ozone amounts to NO_y .

of the TSAM analysis, the baseline adjustment may be viewed simply as forcing the anomaly time series to go roughly through the final MMT estimate at the reference date. The baseline-adjusted IMT estimates employing a reference date of 1980 are presented in the right-hand panels of Figure 9.1. Comparing the left- and right-hand panels of this figure it can be seen that the TSAM analysis has been very effective at providing a common reference for the total ozone time series allowing a clearer comparison of the predicted evolution between models. The baseline-adjusted time series employing a reference date of 1980 show improved agreement with observations for CCMVal-2 relative to CCMVal-1. From the left-hand panels of Figure 9.1 it can be seen that this improvement in CCMVal-2 is fortuitous in that it has not come from a reduction in the spread of models but rather through a more even spread about the observations.

In the two top panels of **Figure 9.2** the 1980 baseline-adjusted MMT estimates (thick grey line) computed in the final step of the TSAM analysis for the 25°S-25°N total column ozone in CCMVal-2 (left) and CCMVal-1 (right) are presented. The 95% confidence and 95% prediction intervals for the MMT estimate are also displayed in these panels as the light and dark-grey shaded intervals respectively and the IMT estimates are superposed on top of the MMT estimate. A comparison of the MMT estimates in this figure reveals a reduced uncertainty and closer agreement with the observations for CCMVal-2 relative to CCMVal-1. The tighter confidence intervals for the CCMVal-2 MMT estimate have two sources. The first is that more models in CCMVal-2 submitted data that extended over a greater portion of the requested period (1960-2100). The second is that several of the models (*e.g.*, AMTRAC3 and WACCM) have improved. In AMTRAC3 the improvements have arisen from the reduction in lower stratospheric chlorine.

The MMT estimates in the upper panels of Figure 9.2 indicate that the evolution of total ozone in the tropics is relatively unchanged between the CCMVal-1 and CCMVal-2 data sets. There is a general decline from the start of the integrations until about the year 2000. Following a gradual increase until about 2050, column ozone amounts decline slightly toward the end of the century. However, after the year 2000, the secular variation in annual mean tropical ozone is only about 10 DU. Increased transport by the BD circulation is likely one of the largest drivers (Shepherd, 2008; Li *et al.*, 2009), and chlorine only has a small influence. The corresponding TSAM analysis of the 50 hPa Cl_y in this latitude band may by found in Figures 9S.5.8 in the supplement to this chapter.

Finally, in the lower panel of Figure 9.2 we consider the impact of using the earlier reference date of 1960 for the baseline-adjustment of total column ozone time series.

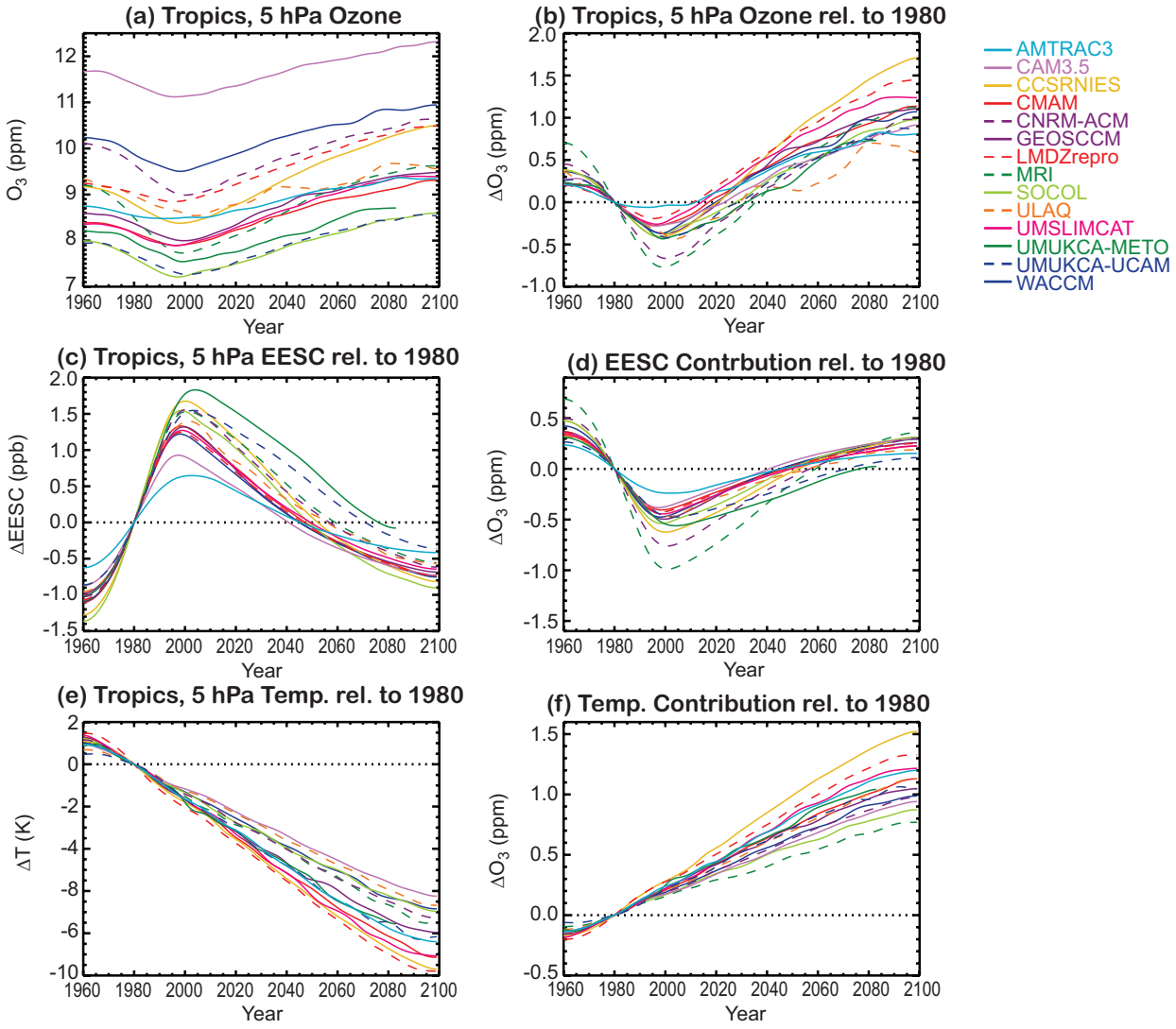

Figure 9.4: Results of the MLR analysis for the CCMVal-2 models in the latitude band 25°S-25°N. (a) Evolution of ozone at 5 hPa, (b) Change in 5 hPa ozone relative to 1980 levels, (c) Evolution of $Cl_y + \alpha Br_y$, (d) Contribution of $Cl_y + \alpha Br_y$ to the ozone change. (e) and (f) are the same as (c) and (d), except for temperature. Curves in this figure were smoothed with a 1:2:1 filter applied iteratively 30 times.

This is only possible for the CCMVal-2 data. It can be seen that the use of an earlier reference date for the pre-ozone-hole baseline causes a significant increase in the spread of the anomaly time series particularly at the time of maximum ozone depletion. Relative to using a 1980 reference date for the baseline adjustment, the use of 1960 causes the MRI and CNRM-ACM to be larger outliers having excessive ozone depletion in all years. SOCOL is an outlier for both 1960 and 1980 baselines after about 2050. This is due to the BD circulation and trend being particularly large in that model, as indicated in Figure 9.6 (see also Chapters 4 and 5). The use of reference dates spanning the range 1970-1980 for both total column ozone and 50 hPa Cl_y is presented in Section 9S.1 of the supplement to this chapter.

9.3.4 Multiple linear regression analysis

Figure 9.3 shows the sensitivity of tropical (25°S - 25°N) ozone to temperature, $Cl_y + 5Br_y$ and NO_y. There is general agreement among models in the middle to upper stratosphere with the exception of MRI and CNRM-ACM, which show higher ozone sensitivities to $Cl_y + \alpha Br_y$, and AMTRAC3 which has more sensitivity to NO_y than most models. The MRI results are consistent with the findings of Chapter 6 showing a much higher than expected ClO/Cl_y ratio. However, at this time it is not clear why CNRM-ACM and AMTRAC3 show these higher sensitivities.

Figures 9.4a and b show the evolution of ozone and its change relative to 1980 at 5 hPa in the tropics (25°S - 25°N). There is a large spread in the time-mean values of

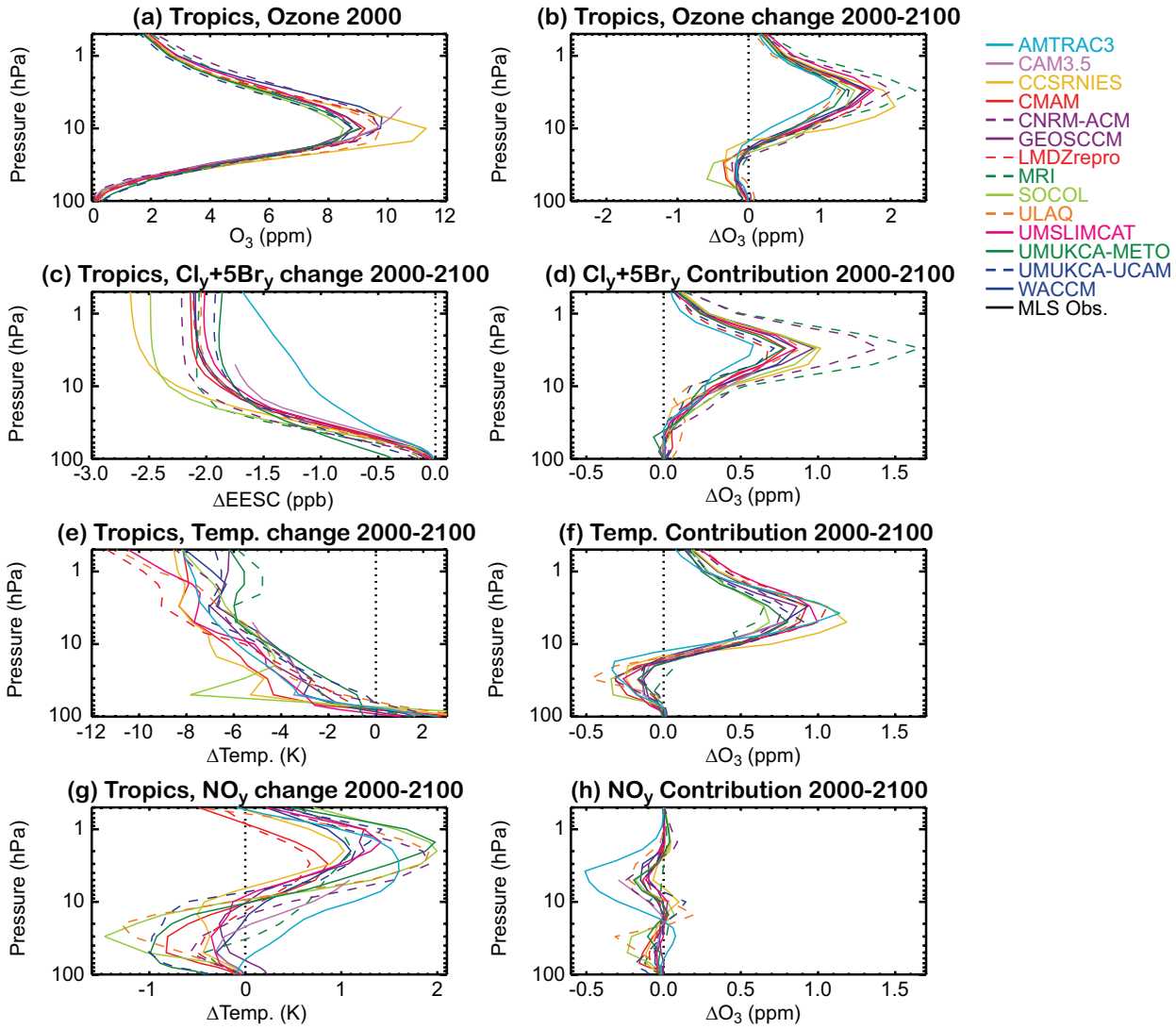

Figure 9.5: Vertical profile results of the MLR analysis for the CCMVal-2 models in the latitude band 25°S-25°N. (a) Ozone in the year 2000, (b) Ozone change from 2000 to 2100, (c) Cl_y + αBr_y change from 2000 to 2100, (d) Contribution of the Cl_y + αBr_y change to the ozone change. (e) and (f) are the same as (c) and (d), except for temperature, and (g) and (h) are the same as (c) and (d), except for NO_y.

ozone, from 8 to 12 ppmv, and the change relative to 1980 levels also varies substantially. Most models show a peak ozone loss of about 0.25 to 0.5 ppmv by the year 2000 and exceed 1980 levels around the year 2020, and 1960 levels by about 2040. MRI and CNRM-ACM have larger than average peak ozone loss, whereas AMTRAC3 has less than average. Generally, those models with a smaller ozone loss recover earlier, and those with a larger loss recover later.

Similar variations can be seen in the change in Cl_y + αBr_y (Figure 9.4c), suggesting that differences in peak ozone loss and date of return to 1960 and 1980 levels can be explained partially by differences in contributions from Cl_y + αBr_y. However, this relationship is not the only relevant factor, as MRI and CNRM-ACM have the largest peak ozone loss, but do not have the largest change in Cl_y + αBr_y. Upper stratospheric ozone is also influenced by temperature, with most models cooling by 7-9 K from 1960-2100. Those models with the largest cooling, 10-11 K (CCSRNIES, CMAM, LMDZrepro, UMSLIMCAT) also have some of the largest temperature contributions to the ozone change. The contributions of Cl_y + αBr_y and temperature to the ozone change, computed from the regression analysis, are shown in Figures 9.4d and f respectively. The term that dominates the trends in ozone at this level varies depending on the time period, but in general Cl_y + αBr_y dominates over the past and beginning of the 21st century, with temperature changes causing the largest ozone changes during the 2nd half of the 21st century. The contributions from NO_y and HO_x under the chosen A1b GHG scenario are negligible in most cases and are not shown.

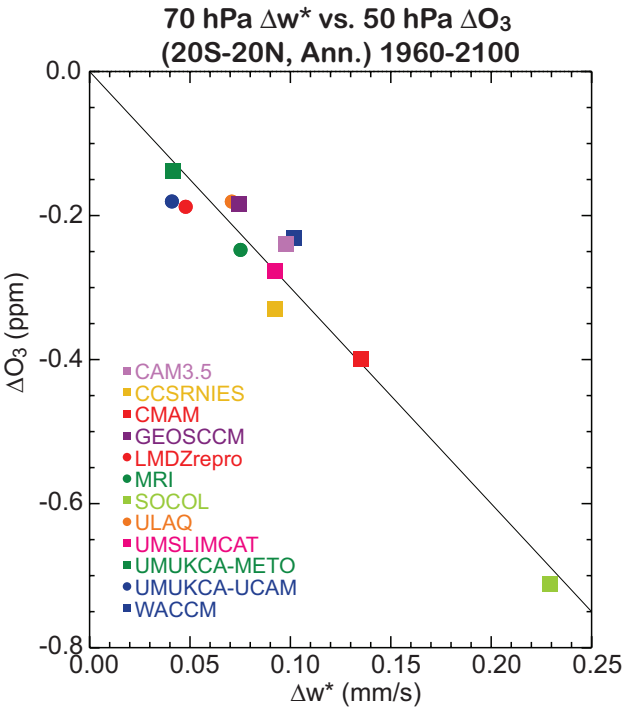

Figure 9.6: Scatter plot showing the differences (from 1960 to 2100) in 70 hPa $\overline{w}^*$ and 50 hPa ozone for those CCMVal-2 models which supplied data. The values are annual averages over the latitude range 25°S-25°N.

The ClO/Cl_y ratio for MRI suggests that the model has much larger amounts of ClO than should be expected (Chapter 6) which leads to the high sensitivity of ozone to $Cl_y + \alpha Br_y$ noted here. The reason for the high sensitivity of CNRM-ACM is not clear. The low $Cl_y + \alpha Br_y$ contribution of AMTRAC3 is due to the parameterisation of Cl_y which is less realistic in the tropical middle stratosphere.

Figure 9.5 shows the results of the MLR analysis for the vertical profile of the ozone change for 2000-2100. The maximum ozone change since 2000 occurs typically at about 3 hPa, with a typical increase of about 1.5 ppmv (Figure 9.5b). Figure 9.5c indicates that in the upper stratosphere of most models, $Cl_y + \alpha Br_y$ decreases by 2 ppbv over this period. CCSRNIES and SOCOL have larger than average decreases in $Cl_y + \alpha Br_y$, and AMTRAC3 has a smaller than average $Cl_y + \alpha Br_y$ change, with a quite different vertical structure for reasons noted previously. Again, MRI and CNRM-ACM have the largest ozone changes due to $Cl_y + \alpha Br_y$ (Figure 9.5d) and AMTRAC3 has a smaller increase. The NO_y increase in most models peaks in the range 1-2 ppbv (Figure 9.5g) and combined with the sensitivities shown in Figure 9.3 most models indicate a very small overall impact on ozone, less than 0.2 ppmv. AMTRAC3 is an exception in showing a much larger impact for reasons that are not clear. Apart from these exceptions, most models show about equal contributions to ozone change from changes in $Cl_y + \alpha Br_y$, temperature and NO_y.

9.3.5 The effect of upwelling on ozone

As indicated in Section 9.2.2, results from MLR are difficult to interpret in the lower stratosphere. Instead we show in **Figure 9.6** the relationship between the change in tropical (25°S - 25°N) ozone at 50 hPa, and the change in the vertical residual velocity, $\overline{w}^*$, at 70 hPa, for the period 1960-2100. All the models for which data were available show an increase in tropical upwelling and a decrease in ozone over this period. A linear regression line through the results goes through the origin, indicating that upwelling is the dominant contributor to ozone reduction at this level. Most models yield an increase in upwelling of 0.04-0.10 mm/s during this period, corresponding to ozone reductions of 0.15-0.35 ppmv. SOCOL is significantly different from the other models in simulating larger increases in upwelling (Chapter 9.3.3 and 4.2.3) and larger ozone losses which both lead to the large cooling seen in Figure 9.5e.

9.3.6 Brief summary

The analysis has shown that the dominant factors that affect ozone evolution in the tropics in the upper stratosphere are changes in $Cl_y + \alpha Br_y$ and temperature. In the lower stratosphere the changes in the evolution of the BD circulation, as diagnosed by an increase in tropical upwelling, are primarily responsible for the modelled ozone changes.

9.4 Mid-Latitude Ozone

9.4.1 From the 2006 WMO assessment:

- In the Northern Hemisphere (NH) column ozone returns to 1980 values by about 2035, well ahead of the return of halogen loading to 1980 values (2035-2050). In the Southern Hemisphere (SH) column ozone returns to 1980 values over the period 2025-2040.
- There is a wide spread in peak Cl_y values simulated for the year 2000.

9.4.2 Further analysis of the CCMVal-1 runs

One of the processes affecting mid-latitude ozone — the increase due to GHG-induced stratospheric cooling — has recently been confirmed as a major process for the mid-latitudes (Waugh *et al.*, 2009). The ozone increase occurs in the upper and middle stratosphere. Using the same model, Li *et al.* (2009) estimated that the climate effect led

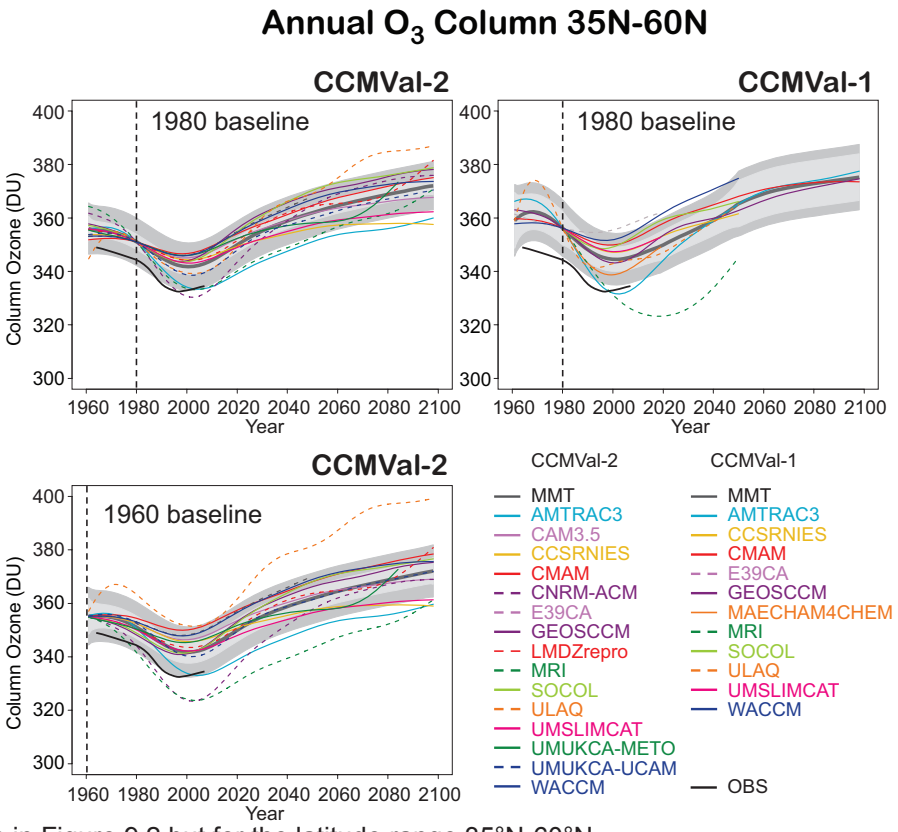

Figure 9.7: As in Figure 9.2 but for the latitude range 35°N-60°N.

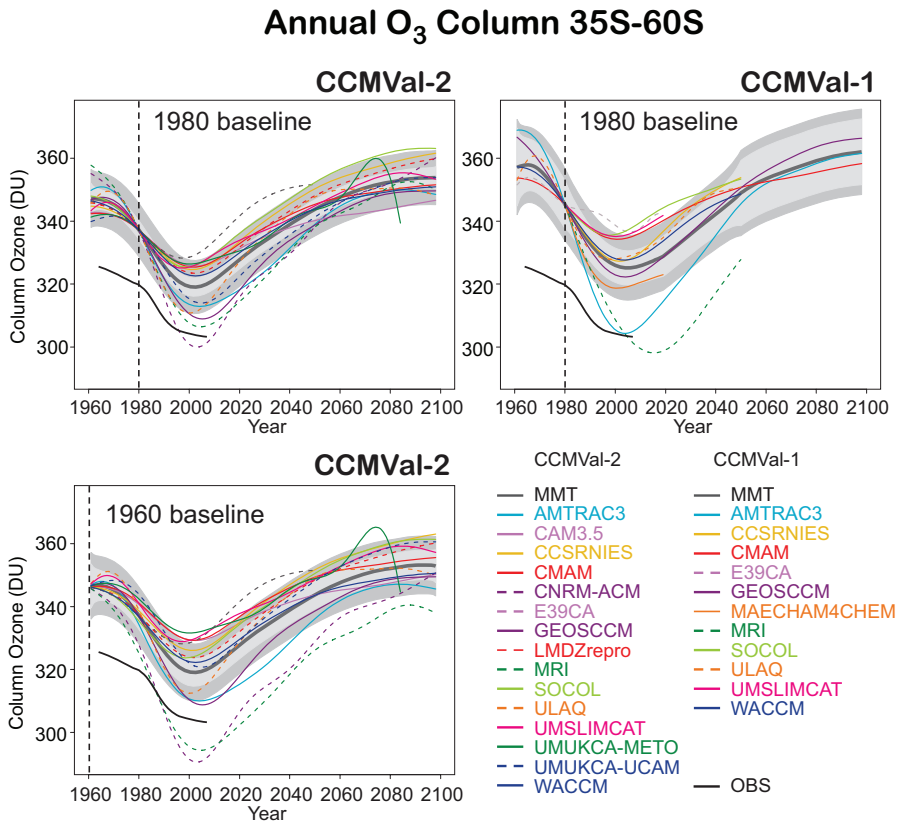

Figure 9.8: As in Figure 9.2 but for the latitude range 35°S-60°S.

to an increase in the extra-tropical ozone column by about 6% in the NH, and about 3% in the SH. These hemispheric differences are likely related to differences in ozone transport.

9.4.3 Mid-Latitude TSAM analysis

In **Figures 9.7** and **9.8**, the 1980 baseline-adjusted IMT and MMT estimates of total column ozone in the latitude bands 35°N-60°N and 35°S-60°S are respectively presented for CCMVal-2 (top left) and CCMVal-1 (top right). These indicate that the multi-model average of total ozone is generally larger than the observations for both CCMVal-1 and CCMVal-2 in these latitude bands with CCMVal-1 displaying the larger error. While the multi-model average of CCMVal-2 more closely corresponds to observations, the raw time series data for both CCMVal-1 and CCMVal-2 show a broad background of total ozone for both hemispheres which spans the range of observations (Figures 9S.9 and 9S.17 of the supplement to the chapter). In both hemispheres, the 1980 baseline-adjusted MMT estimates of ozone indicate that the ozone minimum is reached by roughly the year 2000 and that ozone increases steadily and significantly thereafter. By 2050, northern mid-latitude ozone shows relatively greater increases than southern mid-latitude ozone, probably because of transport from lower latitudes. Other influences such as NO_x- and HO_x-catalysed ozone destruction are likely to have small impacts because the source molecules (N_2O and H_2O) have small trends (Chapter 6).

The 1980 baseline TSAM analysis provides some evidence that improvement has been realised in CCMVal-2 relative to CCMVal-1 with respect to mid-latitude ozone in both hemispheres. Those models which were low outliers in CCMVal-1 for southern latitudes (AMTRAC and MRI) are now more consistent with the other models. The CCMVal-2 1980 baseline analysis in the northern latitudes, however, indicates that these models are at the low end of the range of model results (Figure 9.7), but are consistent with observations from 1980 onwards. The behaviour of the UMUKCA-METO near the end of its IMT estimate (lower panels of Figures 9.7 and 9.8) appears to be an end effect due to an anomalously low data value at the end of its time series in 2084.

In the lower panels of Figures 9.7 and 9.8 the TSAM analysis of mid-latitude ozone employing a 1960 baseline adjustment is presented. The use of the earlier reference date significantly alters the occurrence of outliers in the trend estimates. For example, in both latitude bands, CNRM-ACM and MRI are signicantly low outliers while, in northern latitudes, ULAQ appears as a significant high outlier, with values that greatly exceed all models during the entire period.

In **Figure 9.9** the TSAM analysis for NH mid-latitude

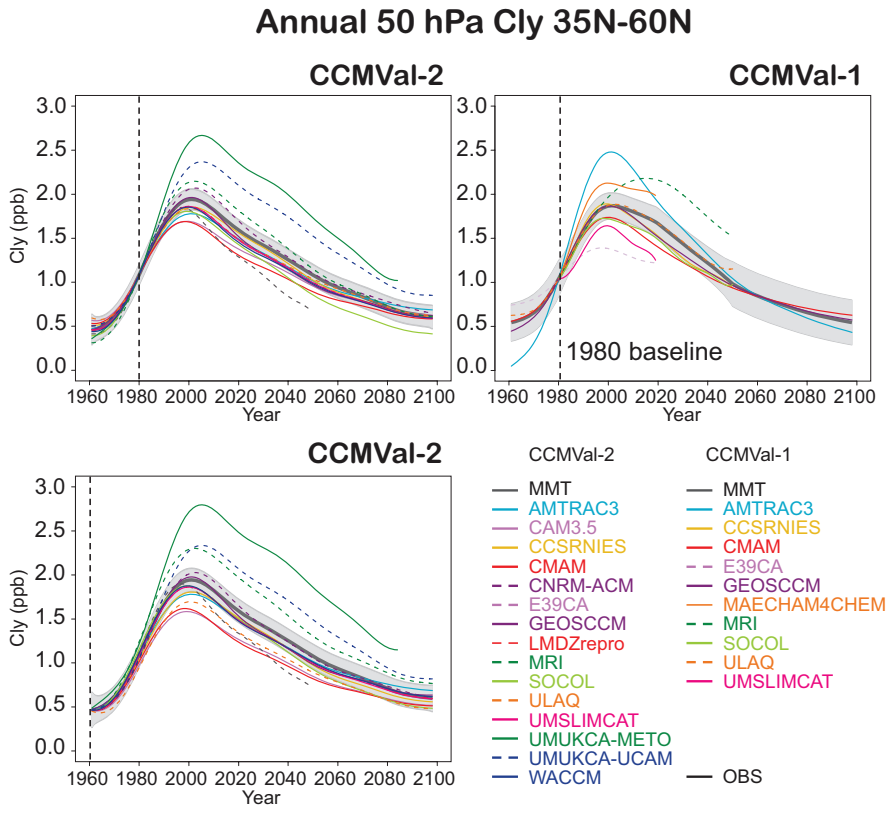

Figure 9.9: As in Figure 9.2 but for 50 hPa Cl_y in the latitude range 35°N-60°N.

50 hPa inorganic chlorine (Cl_y) is presented. The SH Cl_y appears very similar (see Figure 9S.22 of the supplement). Again, there is a large spread in Cl_y, which maximises near the year 2000. The spread between models in CCMVal-1 and CCMVal-2 is roughly equivalent with each having several outliers. The most significant outlier in the CCMVal-2 set is UMUKCA-METO, which has excessive Cl_y in both hemispheres for all years. While the evolution of ozone generally follows that of chlorine (see Section 9.6.4), the specific behaviour of Cl_y for each model does not appear to account for the outliers of total column ozone identified in Figures 9.7 and 9.8.

9.4.4 Multiple linear regression analysis

The evolution of upper stratospheric ozone, and the contributions of the different chemical mechanisms is very similar in mid-latitudes as in the tropics. **Figures 9.10a**, **b** show the vertical profiles of ozone change in midlatitudes (35°S-60°S and 35°N-60°N) over the 21st century. The ozone increases are similar to those obtained in the tropics, but without the loss in the lower stratosphere in most models. The contributions of $Cl_y + \alpha Br_y$ (Figure 9.10c, d) and temperature (Figures 9.10e, f) are also similar to the results obtained in the tropics. Again MRI and CNRM-ACM reveal much larger contributions of $Cl_y + \alpha Br_y$ to the ozone differences, although the AMTRAC3 parameterisation reveals no clear bias in this region. The contribution to ozone change from NO_y (Figures 9.10g, h) is much smaller than the other terms, and the individual models do not show as wide a range.

9.4.5 Brief Summary

The main factors that affect ozone in mid-latitudes are transport (Chapter 5), and the evolution of halogen amounts, particularly during periods of high aerosol loading following volcanic eruptions (see Chapter 8). In addition, GHG cooling of the stratosphere slows chemical destruction rates leading to an increase in ozone, particularly in the upper stratosphere.

9.5 Polar Ozone

9.5.1 From the 2006 WMO assessment:

- Antarctic ozone is strongly anti-correlated with Cl_y amounts.
- Most models simulate a low bias in Antarctic Cl_y which gives rise to an early return of ozone back to 1980 values.
- Arctic ozone returns to 1980 levels before halogen amounts return to 1980 values and ahead of Antarctic ozone. The main influences on ozone include the enhancement of the BD circulation and the slowing of gas-phase ozone loss in the stratosphere by GHG cooling.

9.5.2 Further analysis of the CCMVal-1 runs

Eyring *et al*. (2006) show that the area of the Antarctic ozone hole, based on the fixed 220 DU threshold, is simulated by CCMs to be smaller than observed. Huck *et al*. (2007) propose an improved method for selecting an ozone threshold for delineating the ozone hole. The discrepancy between observations and models has been explained in part by Struthers *et al*. (2009) who show that some models poorly simulate the size of the polar vortex and confirm that the 220 DU contour is not necessarily appropriate for delineating the region of severe ozone depletion in models with systematic ozone biases. Also, according to WMO (2007, Chapter 2, Figure 2-10), the previous simulations (as well as the CCMVal-2 simulations) were completed with bromine concentrations that were probably too low, because of the neglect of very short-lived species.

Eyring *et al*. (2006) show that the interannual variability of the size of the simulated ozone hole was typically over twice that observed, despite the ozone hole being generally smaller. Comparison of AMTRAC experiments for a 15-year overlap period (Austin and Wilson, 2006), indicated that the observed SSTs gave rise to a smaller, more variable ozone hole than calculations using model SSTs. Although this result is certainly model dependent, the likely reason for the difference is that polar processes are affected by El Niños (*e.g*., Manzini *et al*., 2006; Garnkel and Hartman, 2007) that may not be well simulated by coupled ocean-atmosphere models, particularly those with a simplied stratosphere. The implication is that simulations of the ozone hole and the recovery of Antarctic ozone will depend on the performance of the underlying ocean.

The lower stratospheric temperature arises from the net effect of radiative cooling and heating due to GHGs and ozone respectively, and adiabatic warming from the BD circulation. Hence, the net trend in the lower stratospheric temperature, especially in the Arctic will depend critically on the trend in the BD circulation. For a subset of the CCMVal-1 simulations, the orographic gravity wave drag typically contributed about half of the trend in annual mean tropical upwelling (Li *et al*., 2008; McLandress and Shepherd, 2009a; Garcia and Randel, 2008). However, it should be noted that for CCMVal-2 a wide range of results were obtained in examining the full set of simulations (Chapter 4.2.3).

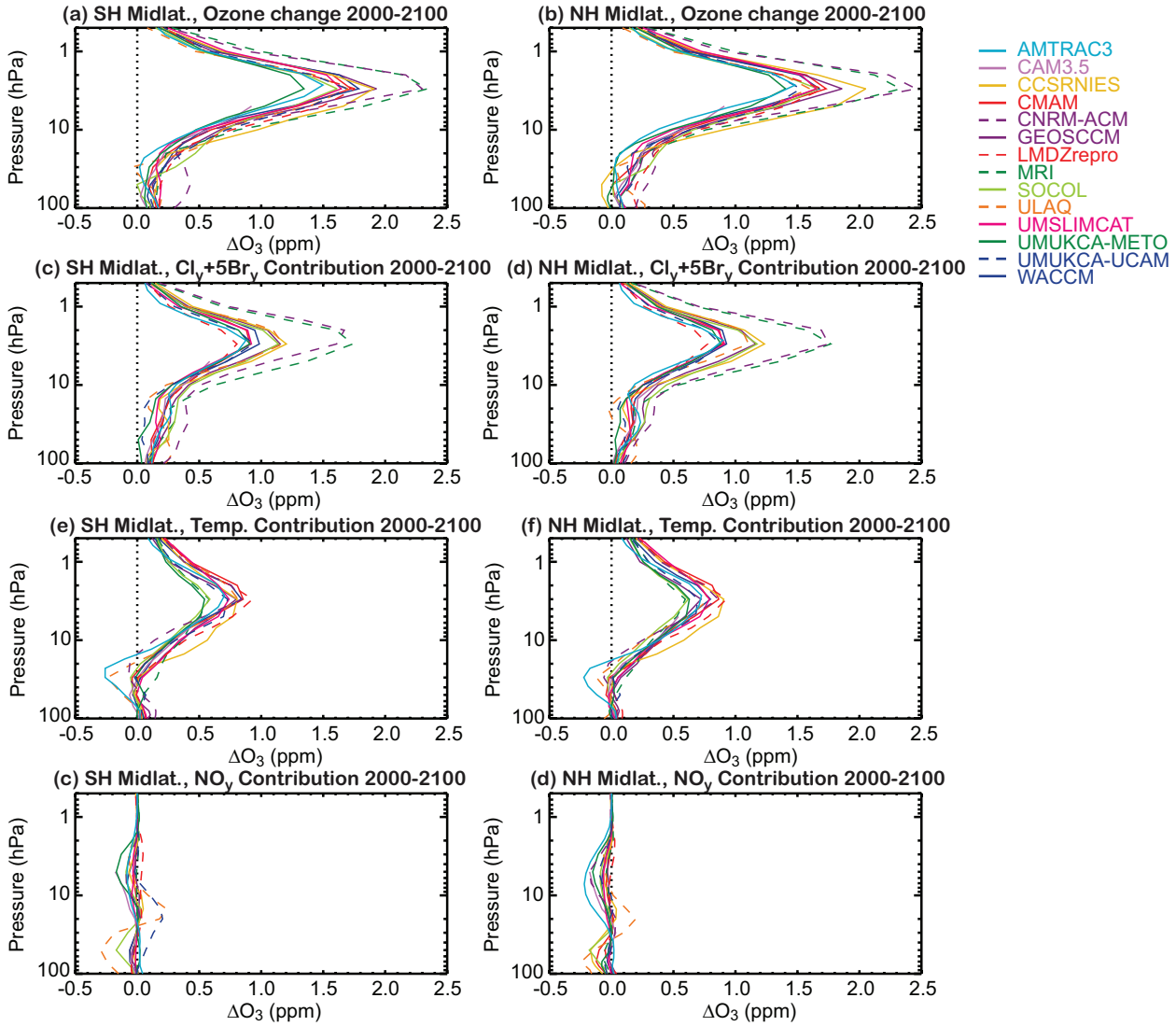

Figure 9.10: Vertical profiles of differences in midlatitude (35°S-60°S and 35°N-60°N) ozone over the the 21st century and the contributions of Cl_y + αBr_y, temperature, and NO_y.

9.5.3 Polar TSAM analysis

The TSAM analyses of spring total column ozone over polar latitudes (60°N-90°N in March and 60°S-90°S in October) are respectively presented in **Figures 9.11** and **9.12**. In Arctic spring, relative to CCMVal-1, CCMVal-2 shows no tendency towards a reduction in model spread (Figure 9S.25 of the supplement). In Antarctic spring, however, the raw time series indicate that the spread of models has increased in CCMVal-2 (Figure 9S.33). This larger spread is associated with a slightly increased negative bias of CMAM relative to its CCMVal-1 contribution, and the inclusion of UMUKCA-UCAM and CAM3.5, which have large positive biases relative to the MMT estimate. This large CCMVal-2 inter-model difference in Antarctic spring background ozone is essentially eliminated in the 1980 baseline-adjusted time series and IMT estimates (Figure 9.12 upper panel and Figs. 9S.33-9S.34). A comparison of the 1980 baseline-adjusted IMT and MMT estimates between CCMVal-1 and CCMVal-2 shows a similar convergence of the models' evolution once the offset in background values of ozone is accounted for (top panels of Figures 9.11 and 9.12), aside from MRI in CCMVal-1.

As was the case for the other latitude bands, employing the earlier reference date of 1960 for the TSAM analysis results in larger inter-model spread for both the Arctic and Antarctic column ozone (lower-left panel of Figures 9.11 and 9.12). Similar to the behaviour in northern midlatitudes, in the Arctic MRI is a low ozone outlier during nearly the entire period (Figure 9.11 and Figures 9S.27-28). In the Antarctic, the use of the earlier 1960 reference date increases the low bias of GEOSCCM, MRI, and

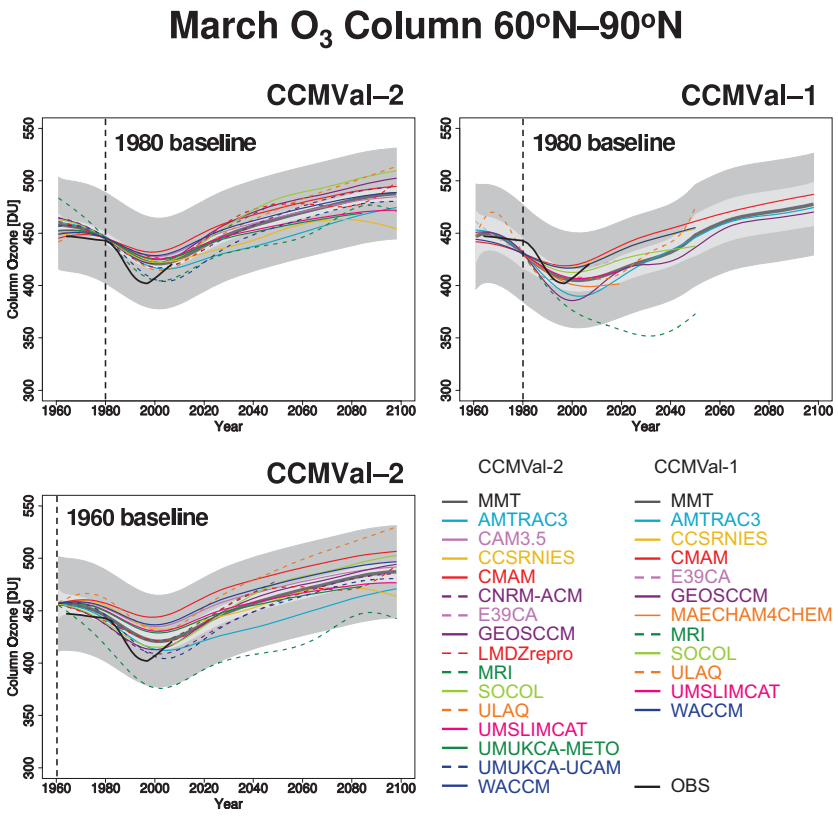

Figure 9.11: As in Figure 9.2 but for the month of March and the latitude range 60°N-90°N.

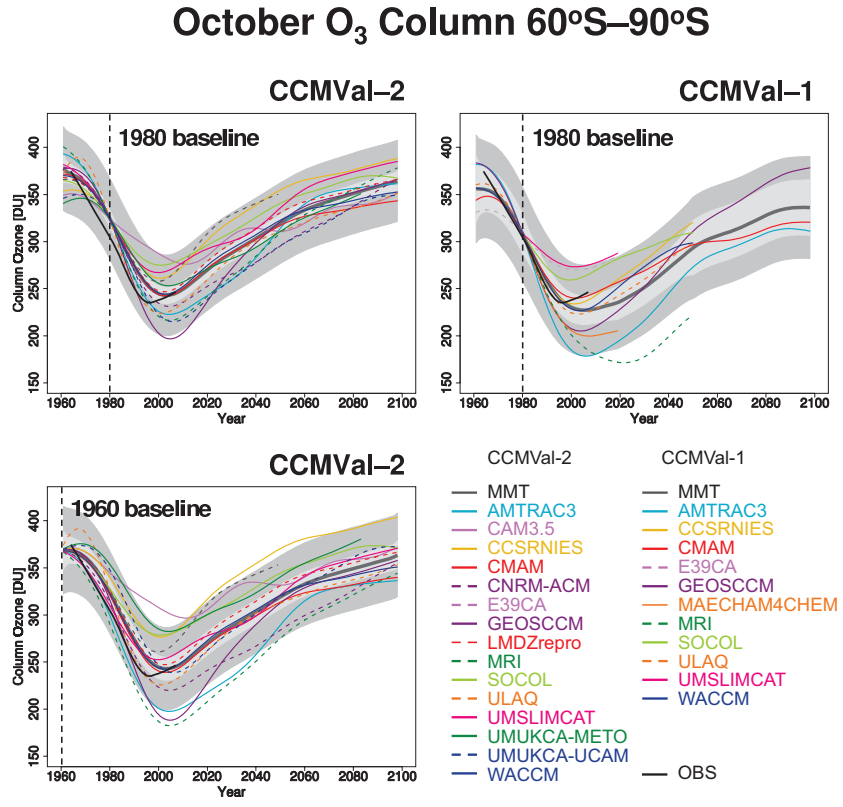

Figure 9.12: As in Figure 9.2 but for the month of October and the latitude range 60°S-90°S.

AMTRAC3 and the high bias of CAM3.5, CCSRNIES, and UMUKCA-METO near 2000. A comparison of the Arctic and Antarctic spring ozone in Figure. 9.11 and 9.12 indicates the tendency for the Arctic ozone to recover earlier than the Antarctic. This will be quantified from the MMT estimates in Section 9.6 of this chapter.

The results for polar regions, particularly Antarctica, are dominated by chlorine amounts. The IMT and MMT estimates of annual 50 hPa Cl_y over polar latitudes (60°N-90°N and 60°S-90°S) are presented in **Figures 9.13** and **9.14**. Aside from the introduction of UMUKCA-METO, and perhaps UMUKCA-CAM, the CCMVal-2 50 hPa Cl_y at both poles shows less spread than CCMVal-1 when a 1980 baseline is employed (upper panels of Figures 9.13 and 9.14). This is primarily associated with improvement in AMTRAC and the absence of MAECHAM4CHEM (see also Figure 5.11 of Chapter 5). These annual means are very similar to the spring means (not shown) in both the Arctic and Antarctic. Unlike ozone, the use of a 1960 baseline in the derivation of the IMT and MMT estimates does not lead to a significant increase in model spread. The general improvement of Cl_y in CCMVal-2 means that individual model results can no longer be as clearly connected with chlorine amount, as was the case for CCMVal-1. Other processes, such as the strength of the circulation and the lower stratospheric temperature, are likely playing a greater role in the precise differences between model results.

9.5.4 Antarctic ozone hole diagnostics

As the Antarctic ozone hole is frequently used as a proxy for ozone depletion, we explore here in more detail its simulation in the CCMVal-2 models. The ozone hole area is investigated, and discussed in relationship to the cold areas simulated by the models as well as other features which affect model performance.

The perimeter of the Antarctic ozone hole has historically been defined as the 220 DU contour, as values this low rarely occurred in measurements and the 220 DU contour was found to lie close to where ozone gradients across the vortex edge were steepest. Once the ozone hole became prominent, such low values became more common in spring. The problems associated with fixed thresholds for denoting the edge of the ozone hole in model simulations has been discussed by other authors (*e.g.*, Huck *et al.*, 2007; Tilmes *et al.*, 2007; Struthers *et al.*, 2009). Those authors supply algorithms for the reanalysis of the ozone hole which might allow for an improved comparison between different model simulations. Generally this requires the availability of extra data such as potential vorticity and also takes into account whether the temperatures in the vortex are low enough for the formation of PSCs, essential to drive the chemistry. Here we explore two particular diagnostics which investigate whether ozone hole differences might be related to ozone biases, or whether ozone hole differences might be related to dynamical representation of the polar vortex.

Figure 9.15a is the zonal-mean ozone over the 10 year period 1996-2005, averaged over the 20 day period centred on the date of the seasonal Antarctic minimum. To reflect actual model characteristics accurately, this date varies according to the model. While several models are close to that observed, several models (UMUKCA-METO, MRI and CCSRNIES) are biased high, although MRI is close to observations near the edge of the classical ozone hole. In Figure 9.15b the zonal average during the peak ozone hole season has been adjusted relative to the minimum daily value attained throughout 60°S-90°S region for the period 1960-1965. Prior to the introduction of satellite based instruments, there was only limited observational coverage of total ozone in high latitudes. Therefore, we take the value of 220 DU as an appropriate minimum for the 1960 to 1965 period. In the case of AMTRAC3 the 1960-1965 minimum poleward of 60°S was 199 DU. The bias is then taken to be 220 - 199 = 21 DU and the curve has been increased by 21 DU to correct for this bias. After applying an appropriate adjustment to each model, the spread in the model results actually increases, but CCSRNIES has improved. This suggests that most models do not have a clear ozone bias which would impede comparison with observations based on a fixed 220 DU threshold.

We now consider whether the location of the polar vortex might be having an influence on the simulated ozone holes. In observations, the maximum gradient in ozone occurs approximately at the edge of the ozone hole, which is related to the edge of the polar vortex (Bodeker *et al.*, 2002; Newman *et al.*, 2007). **Figure 9.16** shows the meridional gradient in total column ozone (1996-2005 average) for each model considered in comparison with observations and it is seen that the simulations place the maximum gradient in different locations. While several models agree well with observations over a wide latitude range, most models place the peak ozone column polewards of that observed (**Figure 9.17**) which may contribute to an ozone hole smaller than observed (as also found *e.g.*, by Struthers *et al.*, 2009). The latitude of the observed maximum gradient is 64.2°S, with a corresponding ozone value of 273 DU (Figure 9.17). By comparison UMUKCA-METO simulates the position and ozone value at the maximum ozone gradient of 68.5°S and 329 DU respectively. Therefore, by reducing the UMUKCA-METO values by 329 - 273 = 56 DU, an alternative estimate for the ozone hole can be determined. Figure 9.15c shows this adjustment of the model results, and the model spread near the edge of the ozone hole has been reduced.

Figure 9.18 shows the ozone hole area for the different definitions considered. Figure 9.18a shows for each

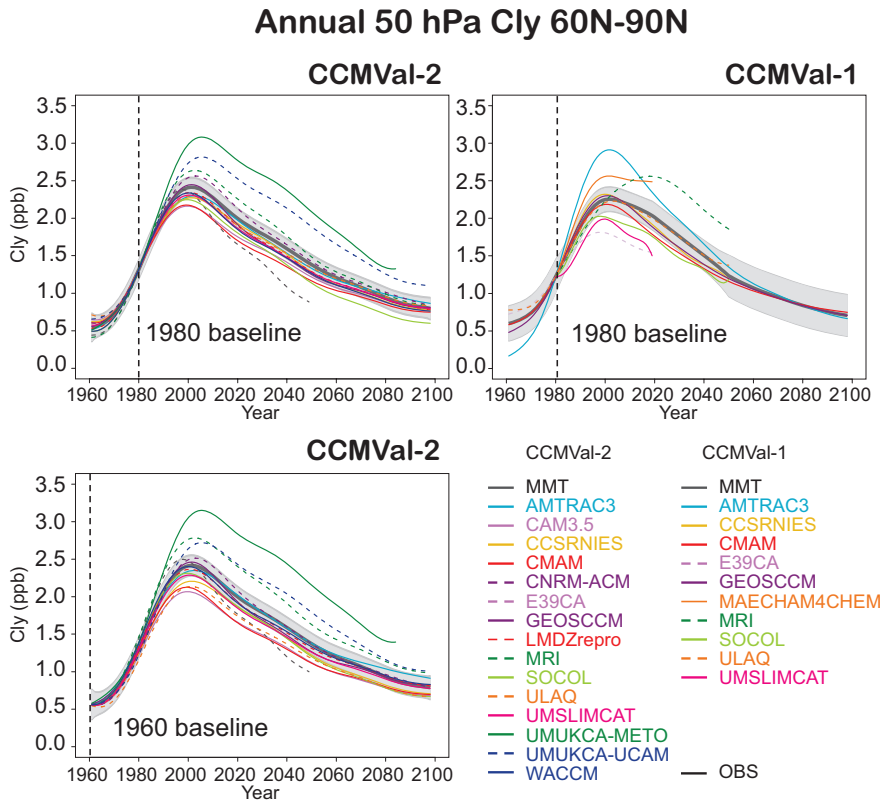

Figure 9.13: As in Figure 9.2 but for 50 hPa Cl_y in the latitude range 60°N-90°N.

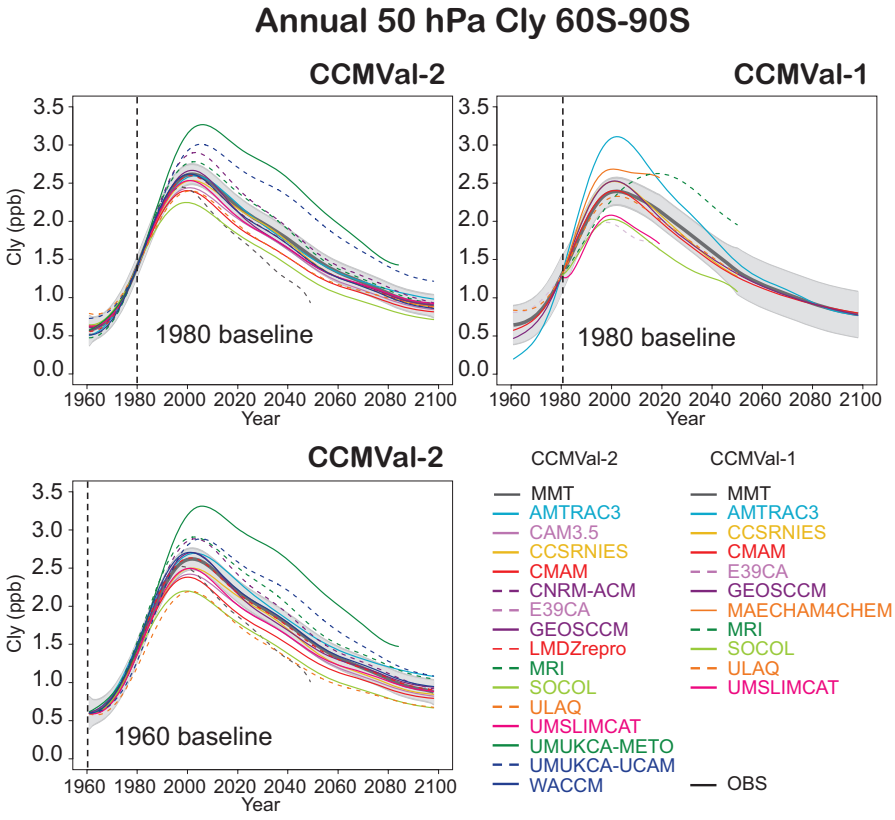

Figure 9.14: As in Figure 9.2 but for 50 hPa Cl_y in the latitude range 60°S-90°S.

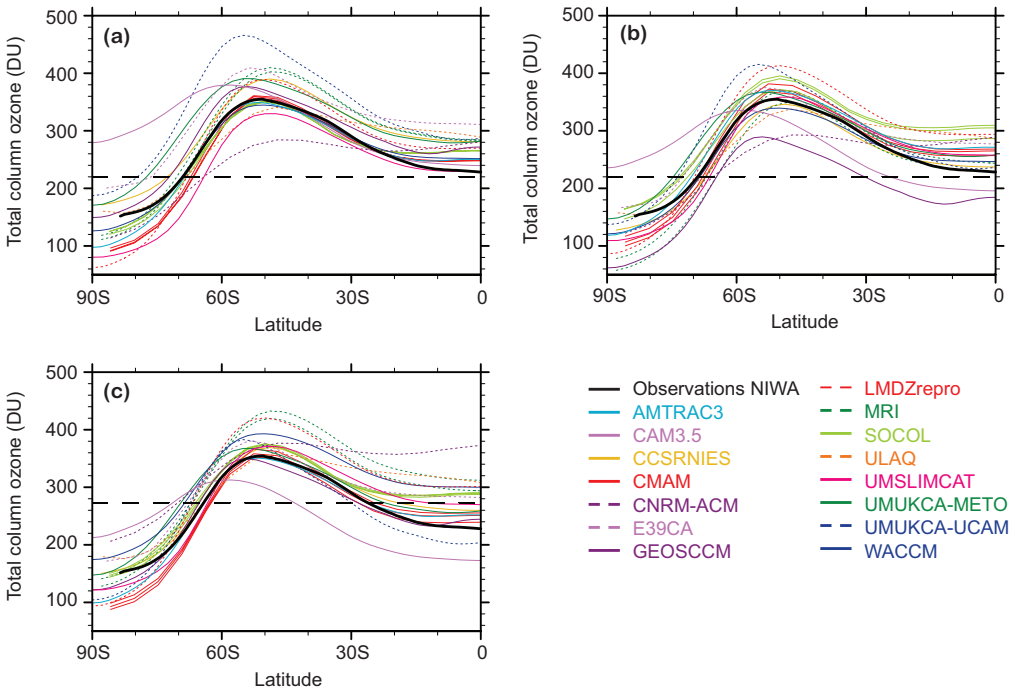

Figure 9.15: Total column ozone as a function of latitude, averaged for the period 1996-2005 for 10 days before and after the minimum column ozone. (a) No adjustments to the model results. (b) Model results have been adjusted relative to the 1960-1965 minimum (see text). (c) Model results have been adjusted relative to the ozone maximum meridional gradient (see text). The results have been obtained from the REF-B2 simulations.

year of the simulations the maximum area for the column ozone less than 220 DU. The agreement with observations is generally poor, with most models under-predicting the size of the ozone hole. If the ozone hole is considered relative to the 1960-1965 minimum, as described for Figure 9.15b, the agreement with observations for several models improves, particularly CCSRNIES and MRI, but SOCOL results are now in poor agreement with observations from 1980 onwards. The improvements arise from the fact that overall these models appear to have a high ozone bias. In comparison SOCOL results are worse under this measure since low ozone occurred in the 1960s due to the dynamics of the model. Figure 9.18c is a measure of the ozone hole relative to the steepest gradients, corresponding to Figure 9.15c. The model simulations are more consistent with each other, primarily because of the substantial correction to the results for UMUKCA-METO. However, most models have ozone holes which remain significantly smaller than observed, by up to 30%. Some models also show very large 'ozone hole' areas prior to 1980 and after 2040 using the steepest gradient criterion. However, there is no implication that the low ozone is necessarily chemistry driven outside the period when halogen levels are expected to be high.

Model Antarctic ozone hole results obtained for the period 1990-2008 for CCMVal-2 (REF-B1) and some statistical comparisons are included in **Tables 9.1** and **9.2**. Compared with observations, most models under-predict the areas of low temperatures (Table 9.1) and therefore the regions of severe ozone depletion are already limited, as shown in Table 9.2. Many models also produce more extreme local ozone loss than observed, since in these models

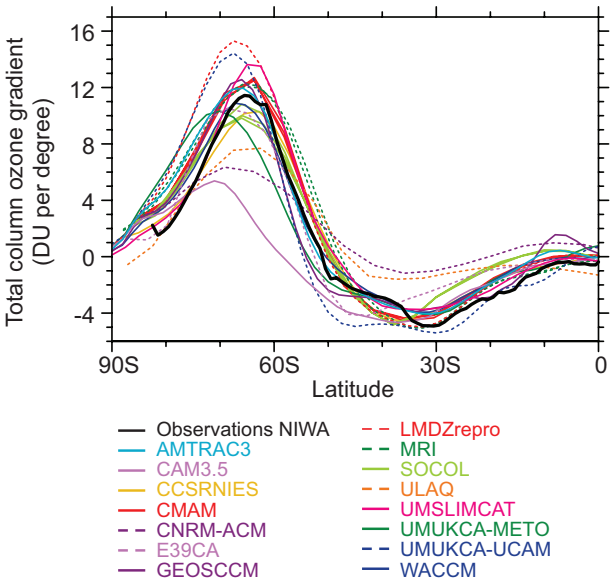

Figure 9.16: Meridional gradient in total column ozone averaged for the period 1996-2005 for the 10 days on either side of the ozone minimum.

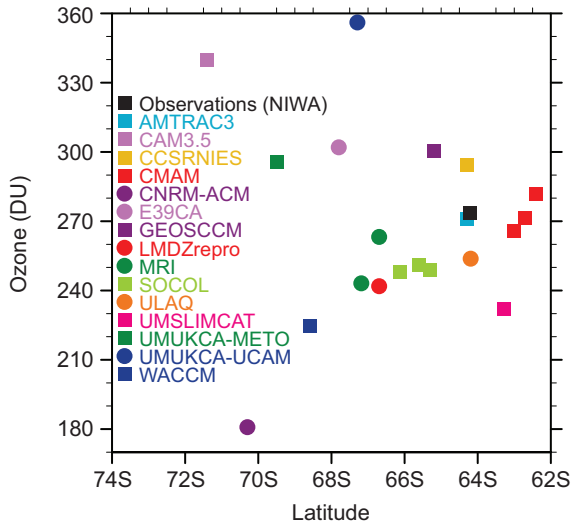

Figure 9.17: Latitude of maximum meridional gradient in total column ozone, as a function of the ozone value at that latitude.

there is a tendency for the ozone hole to extend too high in the atmosphere (not shown). The combination of a low bias in both the ozone minimum and the ozone hole area tends to result in some compensation of errors in the ozone mass deficit, but other models have biases that compound in the ozone mass deficit calculation. Overall, the agreement with observations in most models has not improved appreciably since WMO (2007), despite convergence towards common values for the lower stratospheric Cl_y, and this picture likely remains true regardless of the complexity of the diagnostics adopted. An illustration of the range of results obtained is given by **Figure 9.19**, which shows the mean low temperature (T < 195 K) area averaged for July and September in each of the years 1990-2008 (or the end of the simulation) compared with the area of the ozone hole, based on the 220 DU contour. Almost half the models (AMTRAC3, CMAM, LMDZrepro, NiwaSOCOL, SOCOL, ULAQ, UMSLIMCAT and WACCM) provide a consistent relationship between PSCs (represented by T < 195 K) and the ozone hole, as occurs in the observations. The other models indicate strong biases of background ozone as well as difficulties in simulating sufficient PSCs.

Overall these results suggest that some models do not simulate well the vortex structure, including for example a delay in the final warming (Chapter 4, Pawson *et al.*, 2008). With such a large spread in model results for both 1980 and 2060, predictions of the disappearance of the ozone hole remain unreliable, and in any case, the upper and lower panels of Figure 9.18, indicate that these predictions are likely to be definition dependent.

9.5.5 Brief Summary

The dominant factor which affects ozone evolution in the polar regions is the halogen loading. Although considerable uncertainty still exists in the simulated column ozone trends in the Arctic, models are more consistent

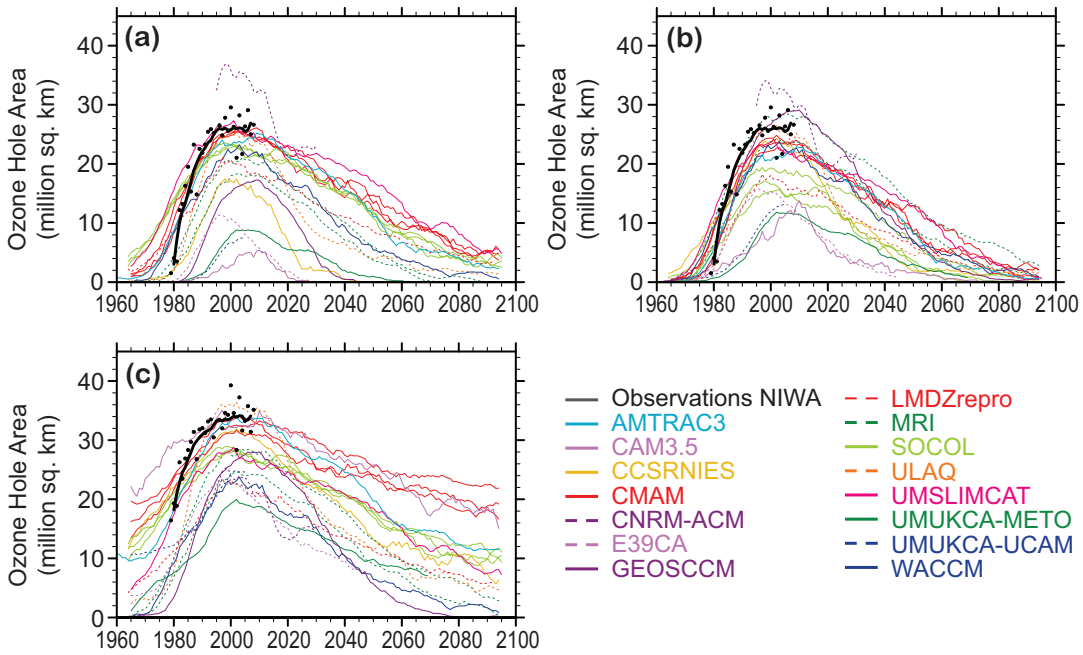

Figure 9.18: Simulated and observed ozone hole areas, based on (a) a fixed, 220 DU amount, (b) the 1960-1965 minimum, and (c) the value at the maximum gradient. The curves indicate 11-year running means of the data for individual years.

Table 9.1: Mean low temperature areas (T < 195 K) for the period July to September for the years 1980-2007 in comparison with observations for the models used in each group of experiments. The uncertainties indicated are approximate 95% confidence intervals for the random error, given by $2s/\sqrt{(n-1)}$,where s is the standard deviation of the annual values and n is the number of years included. The WACCM values are for August and September only.

Model	REF-B1	REF-B2	Model	REF-B1	REF-B2
NCEP data	21.4 ± 0.8	—	LMDZrepro	21.5 ± 0.8	—
AMTRAC3	19.8 ± 0.8	20.4 ± 0.6	MRI	22.6 ± 0.4	22.6 ± 0.5
CAM3.5	17.5 ± 1.5	14.0 ± 1.6	NiwaSOCOL	23.1 ± 0.6	—
CCSRNIES	25.8 ± 0.5	26.4 ± 0.6	SOCOL	21.6 ± 0.4	20.5 ± 0.5
CMAM	19.8 ± 0.6	20.2 ± 0.3	ULAQ	21.7 ± 1.6	21.8 ± 1.5
CNRM-ACM	19.1 ± 1.4	19.3 ± 1.3	UMSLIMCAT	18.9 ± 0.7	19.8 ± 0.9
EMAC	19.0 ± 1.4	—	UMUKCA-METO	14.0 ± 0.8	—
E39CA	24.1 ± 0.7	24.0 ± 0.7	UMUKCA-UCAM	14.7 ± 0.7	16.0 ± 0.6
GEOSCCM	17.5 ± 0.4	—	WACCM	23.9 ± 1.1	21.7 ± 1.6

with each other than in the CCMVal-1 comparisons. Over Antarctica, some models do not simulate well the vortex structure, leading to an ozone hole that is smaller than observed. The ozone hole in many simulations continues to the end of the century.

9.6 Ozone recovery

9.6.1 From the 2006 WMO assessment:

- Full ozone recovery is defined as occurring when ozone depleting substances (ODSs) no longer significantly affect ozone.

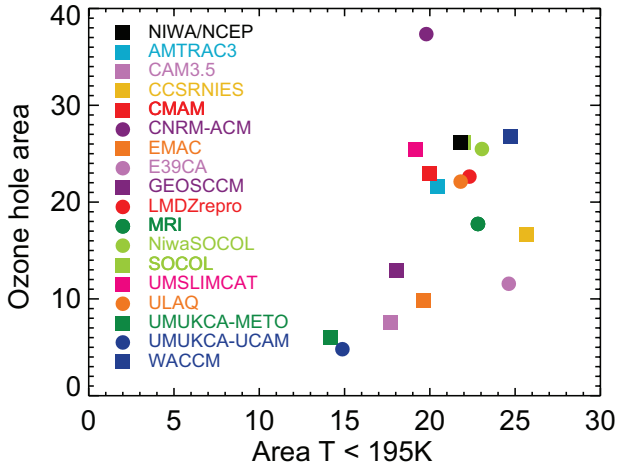

Figure 9.19: Ozone hole area (total column ozone < 220 DU) versus cold area (50 hPa T < 195 K), averaged for July to September for each model compared with observations. The results were calculated from the REF-B1 simulations, and are averaged for the period 1990-2008.

- The return of ozone to 1980 levels is simulated to occur by about 2065 over Antarctica, and up to several decades earlier at other latitudes.

9.6.2 Further analysis of the CCMVal-1 runs

Waugh *et al*. (2009) use simulations of GEOSCCM to examine the impact of climate change on ozone recovery. Waugh *et al*. (2009) conclude that the impact of climate change on ozone recovery depends on the recovery definition and is likely to vary in different atmospheric regions. In particular, for the tropics the total column ozone was found not to return to 1980 values, a commonly used recovery criterion. The results also indicated that full ozone recovery according to the WMO (2007) definition of a negligible impact on ozone due to ODSs would typically not occur before the end of this century.

Austin and Wilson (2006) refer to ozone recovery to 1980 values and suggest that the recovery of the column ozone is advanced relative to Cl_y. This arises from the change in transport, which is larger in the Arctic than in the Antarctic (McLandress and Shepherd, 2009a). Shepherd (2008) and Hitchcock *et al*. (2009) also provide evidence for increased transport effects in the Arctic using temperature and heat flux as a model diagnostic. Possibly related to the increase in the strength of the Brewer-Dobson circulation, simulations also show an increase in stratospheric sudden warmings during the period 1960-2100 of about 50% or more (Charlton-Perez *et al*., 2008; McLandress and Shepherd, 2009b; Chapter 4). This could increase the transport of ozone into the Arctic during winter, as well as increase the interannual variability. Observations of stratospheric sudden warmings are too infrequent and too variable to verify the sudden warming trends obtained in model simulations. An alternative viewpoint is that the increase in

Table 9.2: Commonly used ozone hole diagnostics, averaged over the period 1990-2008, or to the end of the REF-B1 simulations, depending on the model. The uncertainties indicated are approximate 95% confidence intervals for the random error, given by $2s/\sqrt{(n-1)}$, where s is the standard deviation of the annual values and n is the number of years included.

Model	Minimum Antarctic ozone (DU)	Maximum ozone hole area (10^6 km^2)	Ozone mass deficit (Mt)
NIWA data	103 ± 6	26.1 ± 1.2	22.0 ± 2.7
AMTRAC3	74 ± 8	21.8 ± 1.8	24.4 ± 3.8
CAM3.5	187 ± 19	7.5 ± 2.5	1.1 ± 0.5
CCSRNIES	148 ± 10	16.9 ± 2.3	6.6 ± 2.1
CMAM	79 ± 6	23.2 ± 0.8	25.2 ± 2.2
CNRM-ACM	63 ± 4	38.2 ± 3.5	42.4 ± 4.1
EMAC	167 ± 16	10.6 ± 2.5	2.6 ± 1.6
E39CA	121 ± 12	11.7 ± 1.6	3.7 ± 1.1
GEOSCCM	139 ± 8	13.4 ± 1.3	4.6 ± 1.1
LMDZrepro	48 ± 3	22.9 ± 1.1	31.0 ± 2.5
MRI	97 ± 3	14.7 ± 0.6	14.2 ± 1.2
NiwaSOCOL	92 ± 6	26.0 ± 1.6	28.2 ± 3.7
SOCOL	95 ± 4	26.6 ± 0.8	28.7 ± 2.4
ULAQ	102 ± 7	22.5 ± 2.2	15.2 ± 3.4
UMSLIMCAT	79 ± 4	25.0 ± 1.3	34.8 ± 3.5
UMUKCA-METO	168 ± 16	6.2 ± 2.0	2.2 ± 1.1
UMUKCA-UCAM	172 ± 8	5.0 ± 0.8	0.9 ± 0.4
WACCM	101 ± 7	26.4 ± 2.3	22.9 ± 4.3

stratospheric sudden warmings seen in some models over century time scales is representative of a change in climatological state and hence transport effects are relatively unaffected by climate change, apart from the steady increase in the BD circulation (McLandress and Shepherd, 2009b).

9.6.3 Recovery based on TSAM analysis

The IMT and MMT estimates for total ozone and 50 hPa Cl_y presented in Sections 9.3-9.5 may be used to provide individual model, and multi-model estimates of the return to levels associated with a specified reference date. Because the IMT and MMT estimates are smooth curves by construction, the value of ozone and Cl_y for any reference date prior to maximum ozone depletion may be mapped onto a future date based on the return of ozone or Cl_y to the reference date value. The TSAM analysis, therefore, allows the definition of return dates for a continuous set of reference dates. In order to compare recovery predictions from CCMVal-1 with CCMVal-2, we first consider the commonly used reference date of 1980.

Summary diagnostics of total ozone and 50 hPa Cl_y 1980 return dates for the latitude bands discussed in Sections 9.3-9.5 are presented in **Figures 9.20** and **9.21** respectively. In each latitude band, CCMVal-1 return dates are shown on the left and CCMVal-2 return dates are shown on the right. The MMT estimate of return dates is indicated by large black triangles. Error bars on these estimates are associated with the 95% confidence intervals. These two figures provide a concise summary of the ozone and Cl_y discussed in the previous three sections. They allow an overall comparison of CCMVal-1 with CCMVal-2 through the MMT estimates, the change in individual model predictions to be tracked across the two inter-comparison projects, and the comparison of model predictions with the MMT estimates and with each other for each of CCMVal-1 and CCMVal-2.

Initial inspection of these two figures reveals that return dates for Cl_y are more symmetric in latitude, and more certain, than ozone for both CCMVal-1 and CCMVal-2. In general, return dates for Cl_y are very similar between CCMVal-1 and CCMVal-2 being well within the uncertainty bounds of each. Return dates for total ozone, on the other hand, are not symmetric in latitude and, in the tropics not realised by the MMT estimate at all in CCMVal-2. While the CCMVal-1 and CCMVal-2 MMT estimates of return dates for spring polar and annual mid-latitude ozone are seen to be within each other's uncertainty bounds, those for CCMVal-2 appear to be systematically earlier than CCMVal-1. For example, the spring Arctic ozone recovery to 1980 levels is predicted from the MMT estimate to occur near 2025 for CCMVal-2 (2039 for CCMVal-1) while the Antarctic recovery to 1980 levels is predicted to occur much later near 2052 for CCMVal-2 (2062 for CCMVal-1). The asymmetric structure of polar ozone recovery in Figure 9.20 is an indication that, in addition to Cl_y abundance, ozone is affected by dynamical and radiative changes brought about by increased GHG forcing and these have been consistently reproduced in the MMT estimates between CCMVal-1 and CCMVal-2.

In **Figures 9.22** and **9.23** we compare estimates of the return dates to 1960 and 1980 levels for total ozone and 50 hPa Cl_y respectively. In general, the return date for ozone is longer when the earlier reference date of 1960 is used (Figure 9.22). In particular the Antarctic return date changes significantly, from roughly 2055 to nearly 2100. From Figure 9.23 it appears that 50 hPa Cl_y does not return to its 1960 value by the end of the 21st century outside the tropics. Appealing to the earlier reference date of 1960 therefore has significant impact on return dates. However, it must be noted that the use of 1960 as a reference date for the CCMVal-2 comes at the beginning of the time series for many models and some of the sensitivity found here

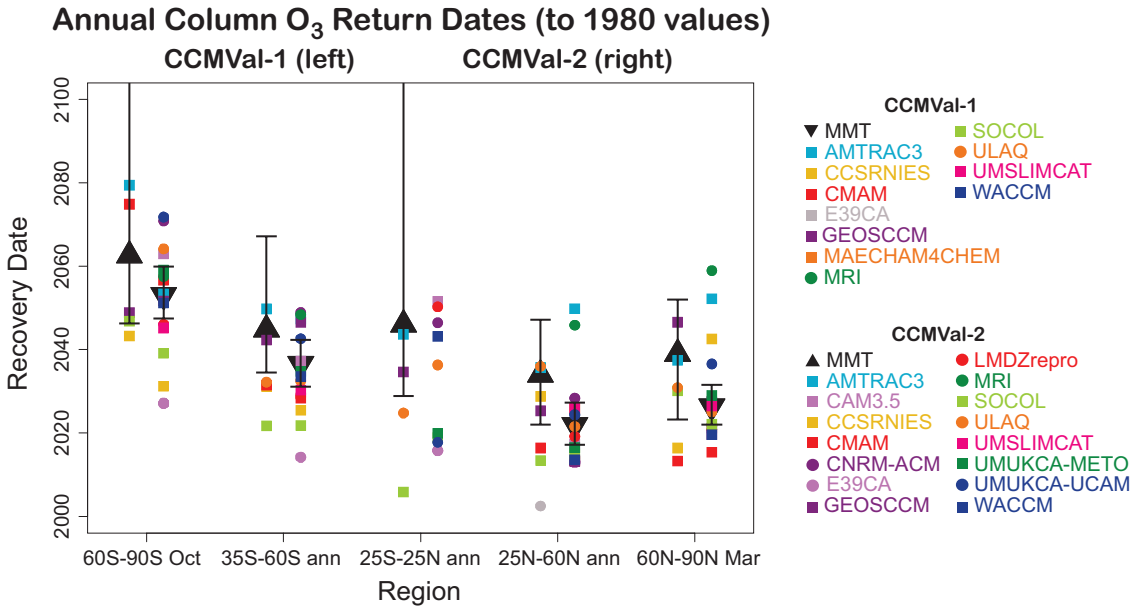

Figure 9.20: Date of return to 1980 values for the annual average (tropical and mid-latitude) and spring (polar) total ozone column derived from the IMT (coloured symbols) and MMT (large black triangles) estimates for CCMVal-1 and CCMVal-2 (left and right respectively in each latitude band). The error bars on the MMT estimate of return date is derived from the 95% confidence interval of the MMT estimates to the 1980 baseline-adjusted time series data.

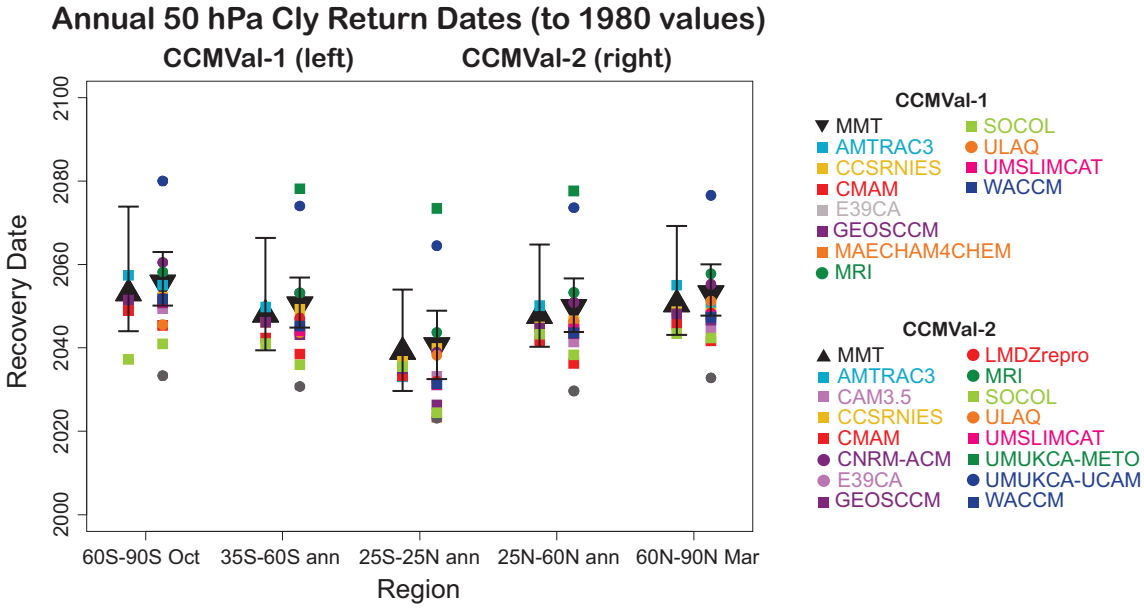

Figure 9.21: Date of return to 1980 values for the annual average 50 hPa Cl_y derived from the IMT (coloured symbols) and MMT (large black triangles) estimates for CCMVal-1 and CCMVal-2 (left and right respectively in each latitude band). The error bars on the MMT estimate of return date is derived from the 95% confidence interval of the MMT estimates to the 1980 baseline-adjusted time series data.

may be associated with spin-up issues at the beginning of the simulations. For example, a number of the models display increasing ozone in the early 1960s prior to their initial decrease in the 1970s and 1980s (*e.g.*, see Figures 9.8 and 9.12). In these models ozone returns to 1960 values both prior to, and after the main loss near year 2000. In these cases the earlier return date was discarded and the later value used. This would appear to be a spin-up issue, or the effect of aerosols following the eruption of Agung (Chapter 8) in these models, suggesting that future experiments should perhaps start even earlier than the period prescribed for CCMVal-2.

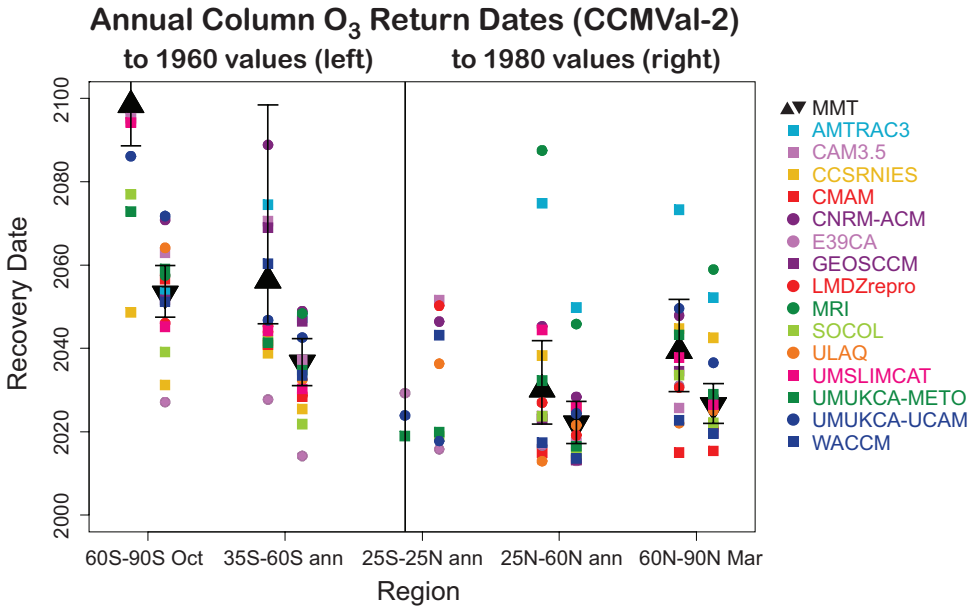

Figure 9.22: Date of return to 1960 (left) and 1980 (right) values for the annual average (tropical and mid-latitude) and spring (polar) total ozone column derived from the IMT (coloured symbols) and MMT (large black triangles) estimates for CCMVal-2. Error bars are as in Figure 9.20.

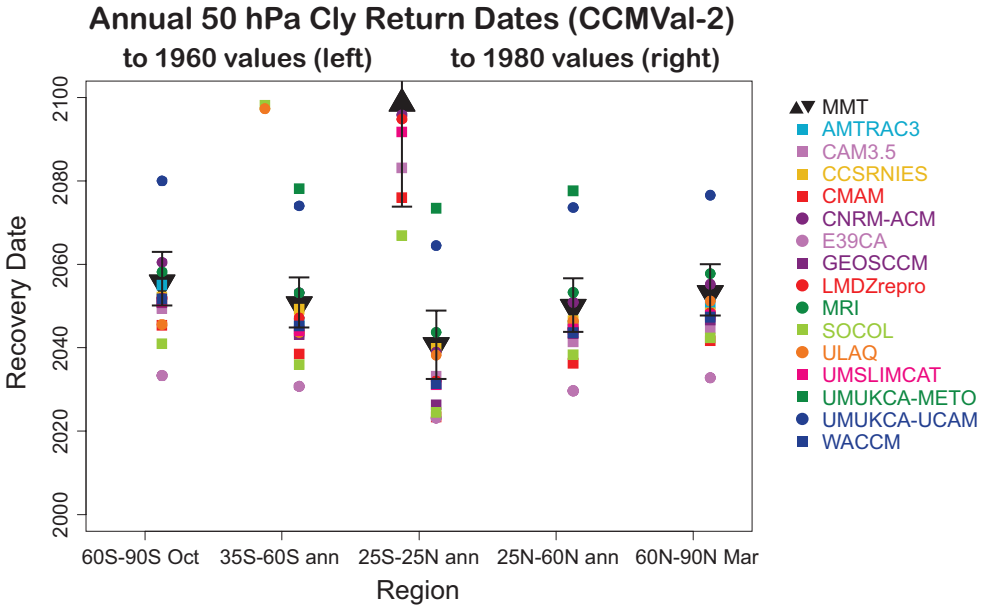

Figure 9.23: Date of return to 1960 (left) and 1980 (right) values for the annual average 50 hPa Cl_y derived from the IMT (coloured symbols) and MMT (large black triangles) estimates for CCMVal-2. Error bars are as in Figure 9.21.

9.6.4 The relationship between O_3 and Cl_y return dates

Figure 9.24 shows the relationship between return date of 50hPa Cl_y and column ozone back to their 1980 values using the MMT results of section 9.6.3. For the Antarctic spring, the models roughly scatter evenly about a similar date for the return of ozone and chlorine to 1980 values (given by the black line), indicating that halogen chemistry is the dominant driver in determining ozone recovery. Several models (CCSRNIES, UMUKCA-UCAM) fall significantly above the line, implying ozone returns faster than Cl_y, and several others fall significantly below the line, implying that ozone returns more slowly than Cl_y. The reason for these differences has not been identified, but may reflect, in part, the fact that in most models ozone recovers slowly in the middle 21st century, and a small change in the reference date (for example 1980 to 1985)

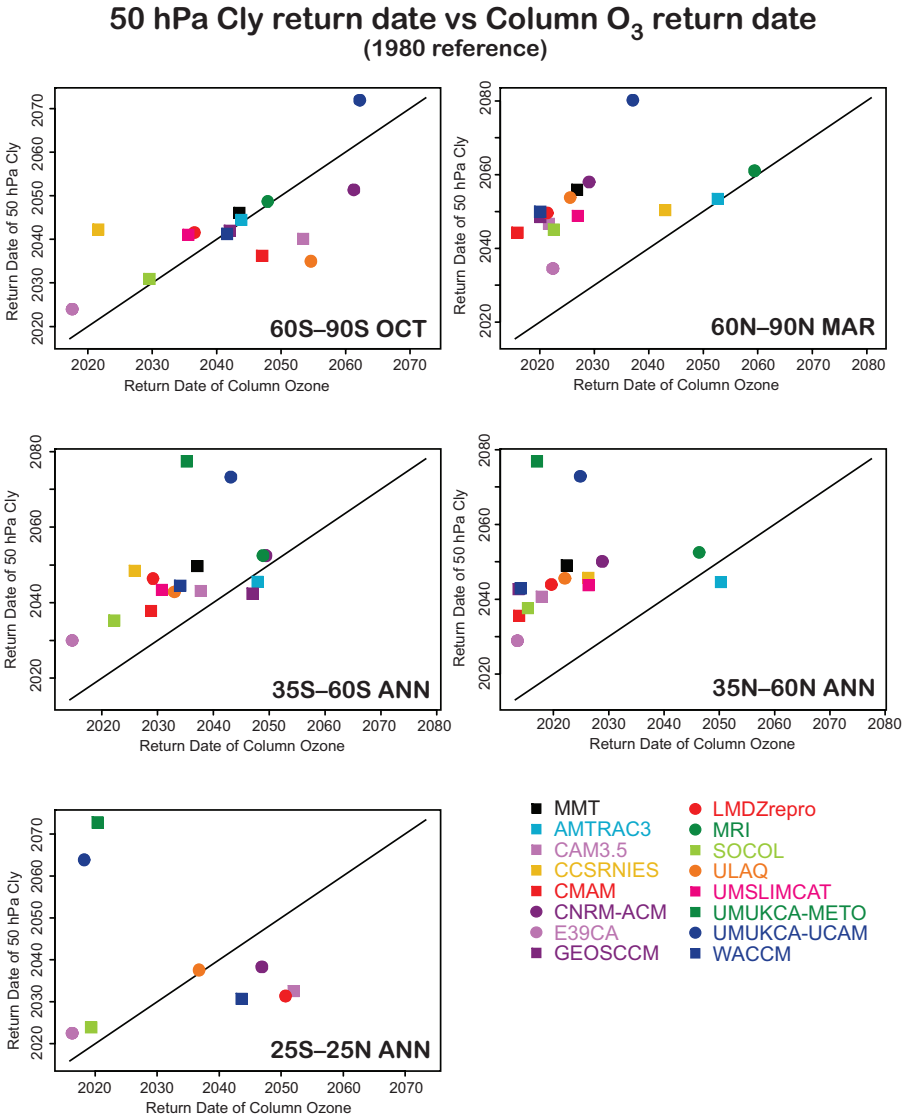

Figure 9.24: Relationship between the date of return of Cl_y to the1980 value compared with the date of return of column ozone for the selected latitude ranges in Figure 9.20. Results are taken from the IMT and MMT fits.

can cause a large change in ozone return date. A different picture is seen for the Arctic spring, and annual mean mid-latitudes where most models return to 1980 column ozone values before Cl_y returns to 1980 values. As indicated in Section 9.6.3, only about half of the models indicate a return of tropical ozone to the 1980 values.

9.6.5 Ozone recovery as a function of latitude and reference year

A complementary view of ozone recovery is shown in **Figure 9.25**, which indicates the return date for the annual mean column ozone appropriate to the reference date given on the abscissa. The column has been separated into two regions, above and below 20 hPa, and the analysis excludes the atmosphere below 500 hPa. For each year in the analysis, the first date after the year 2005 that the ozone partial column returned to the value on the reference date was determined for the mean model results. Above 20 hPa (Figure 9.25, upper panel), ozone recovery is simulated to occur steadily. In this region, the temperature and halogen effects on ozone dominate, as shown by the MLR analysis for the different regions described in the earlier sections. As suggested by this analysis, ozone change is approximately linearly dependent on $Cl_y + \alpha Br_y$. Taking approximate values for $Cl_y + \alpha Br_y$ of 3, 1.5 and 0.75 for 2000, 1980 and 1960 implies that the ozone recovery to 1960 levels should take about 50% longer than the recovery to 1980 levels. This is confirmed by Figure 9.25 (upper panel).

In the lower stratosphere (Figure 9.25, middle panel) a return date could not be established for the tropics due to the strengthening BD circulation which systematically

decreases tropical ozone as the simulations proceed (*e.g.*, Waugh *et al.*, 2009). The results also show a strong hemispheric asymmetry discussed above, with Antarctic ozone recovering much more slowly than Arctic ozone. Again, this is largely due to the increased BD circulation, which for the models as a whole has much more influence in the northern than the southern hemisphere (Austin and Wilson, 2006; Eyring *et al.*, 2007; Shepherd *et al.*, 2008). In high southern latitudes, the simulations on average do not return to the pre-1970 ozone levels before the end of the simulations.

The results for the total column (Figure 9.25, lower panel) combine the results for the two regions. In the tropics, the total ozone column recovers until about 2050 (Figure 9.2) due to decreasing halogen amounts and stratospheric cooling, but thereafter ozone decreases due to the increasing BD circulation. This implies that in the tropics, the total ozone column does not return to pre-1985 values before the end of the simulations. Over Antarctica, recovery to 1960s levels of total ozone does not occur in the mean model until shortly before the end of the simulations.

9.6.6 The Role of transport in mid-latitude ozone recovery

Given the important effects that changes in the BD circulation can have on projected ozone recovery, changes in the seasonal cycle in the different CCMVal models have been analysed with an emphasis on how the spring buildup of ozone relates to ozone recovery. An eight-term harmonic function (plus an extra term for the annual average) was fitted to the zonally and monthly averaged ozone column over mid-latitude bands in each hemisphere for the periods 1960-1979 and 2040-2059. The annual cycle derived from the fitting, with the annual mean for each model and time period removed, and the change in the seasonal cycle is shown in **Figure 9.26**. These results are outside the ozone hole period and show in both hemispheres a maximum in spring and a minimum in autumn. Several models (notably ULAQ, GEOSCCM, CMAM and, to a lesser extent, WACCM) show an increased build-up of ozone through the boreal spring between the 1960-1979 and 2040-2059 periods (panel c). In contrast, other models (AMTRAC3, MRI and UMUKCA-METO) show little change in the amplitude of the seasonal cycle between these periods.

As shown in **Figure 9.27**, changes in the seasonal cycle, as measured here by the change in the amplitude of the seasonal cycle averaged over January-April, show some correlation with the MMT estimate of 1980 recovery date for annual ozone derived from the TSAM analysis (Figure 9.20). The models showing an increased build-up of ozone through the spring have ozone recovery dates for the 35°N-60°N region before 2020. While the models showing little change in the amplitude of the seasonal cycle have

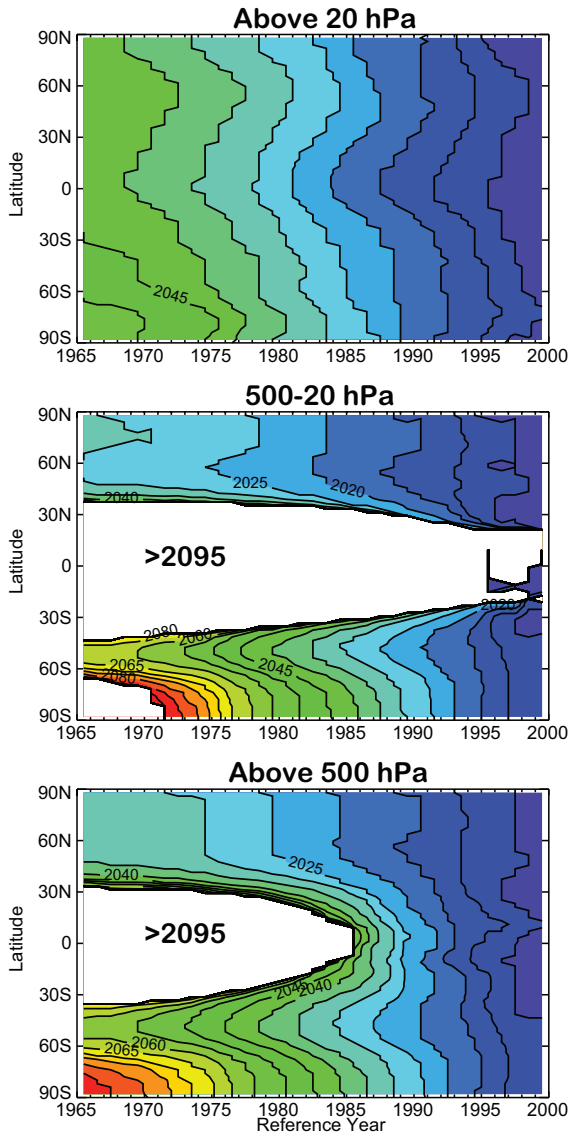

Figure 9.25: Date of return of the annual mean ozone to the value appropriate to the reference year indicated on the abscissa. Results were taken from the models AMTRAC3, CAM3.5, CCSRNIES, CMAM, CNRM-ACM, GEOSCCM, LMDZrepro, MRI, SOCOL, ULAQ, UMSLIMCAT, UMUKCA-UCAM, UMUKCA-METO and WACCM, which were first interpolated to a common latitudinal grid (AMTRAC3). The mean model result was then smoothed with an 11-year running mean filter. Data prior to 1965 (which limits the definition of the reference year data) or after 2094 (which limits the data for the return year) do not exist because of the need for an accurate time-smoothed field. The white region in the figure indicates where the mean model ozone has not recovered by the end of the simulations (nominally 2094). Results are shown for the total column above 500 hPa, for the range 500-20 hPa and for the column above 20 hPa.

recovery dates between 2040 and 2050. The UMUKCA-METO model is an exception, showing little change in the amplitude of the seasonal cycle yet having a recovery date before 2020.

Several models (CNRM-ACM, MRI and UMSLIMCAT) show an increased buildup of ozone during SH late-fall and winter (May, June and July) in the 2040-2059 period (Figure 9.26f), but no coherent changes persist into the spring. The seasonal cycle is further perturbed with the breakup of the Antarctic vortex in October and November, mixing ozone depleted air from within the Antarctic vortex into mid-latitudes. As shown in Figure 9.27, no clear relationship can be found between changes in the spring-time buildup of ozone and the recovery date. The lack of a clear signal in the amplitude of the seasonal cycle of column ozone is further evidence of a weaker change in the SH branch of the BD circulation.

Although chemistry is always a factor affecting the distribution of ozone, the spring-time build-up of ozone is a feature in the annual cycle driven by the transport of ozone from tropical to mid-latitudes by the BD circulation (*e.g.*, Fusco and Salby, 1999; Fioletov and Shepherd, 2003). Analysing the spring-time buildup should, therefore, highlight the role of dynamics over chemistry. Further, we analyse changes in the seasonal cycle over 1960-1979 to 2040-2059 to avoid the period of time when halogens are expected to have the largest effects on column ozone. For these reasons we believe that changes in the spring-time ozone column analysed here are indicative of changes in transport by the BD circulation in the models.

9.6.7 Brief Summary

The main processes influencing total ozone recovery are the increasing strength of the BD circulation, the GHG induced stratospheric cooling and the halogen loading. Because of the lesser importance of the BD circulation in the SH, recovery approximately follows that of Cl_y, while in the NH, the BD circulation and cooling play important roles in speeding up recovery. CCMVal-2 results suggest in general an earlier recovery than the CCMVal-1 results. However, in the tropics, the impact of the BD circulation is such that column ozone does not recover to the values present prior to about 1985 regardless of the reduction in halogen amounts. Nonetheless, the model results continue to show a very wide range of results for the ozone recovery time scale. Finally, because ozone approximately follows Cl_y over the Antarctic, the disappearance of the ozone hole does not occur by the end of the simulation in some models.

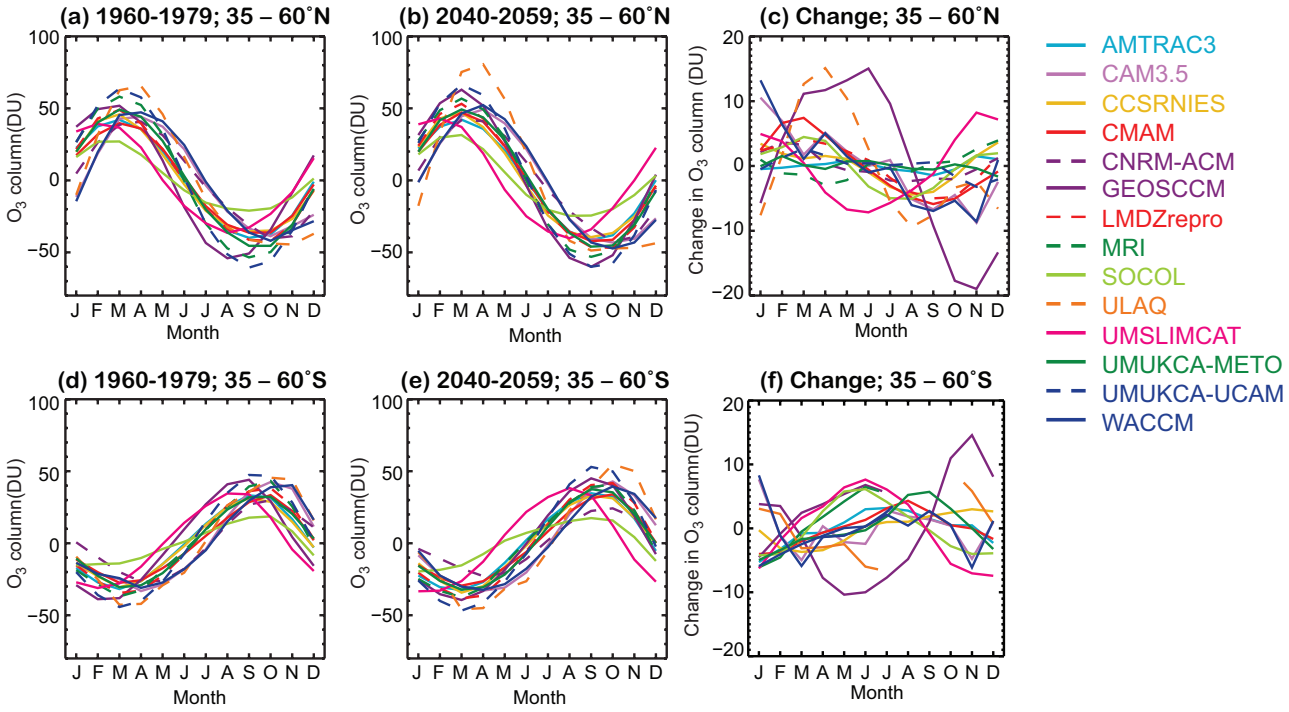

Figure 9.26: The average seasonal cycle of total column ozone over NH and SH mid-latitudes for two periods and its change. (a) 1960-1979, 35°N-60°N, (b) 2040-2059, 35°N-60°N, (c) Change from 1960-1979 to 2050-2059. (d)-(f), as(a)-(c), but for the southern mid-latitudes. Note that the annual mean for each model and each time period is removed from the annual cycle before plotting and before taking the difference.

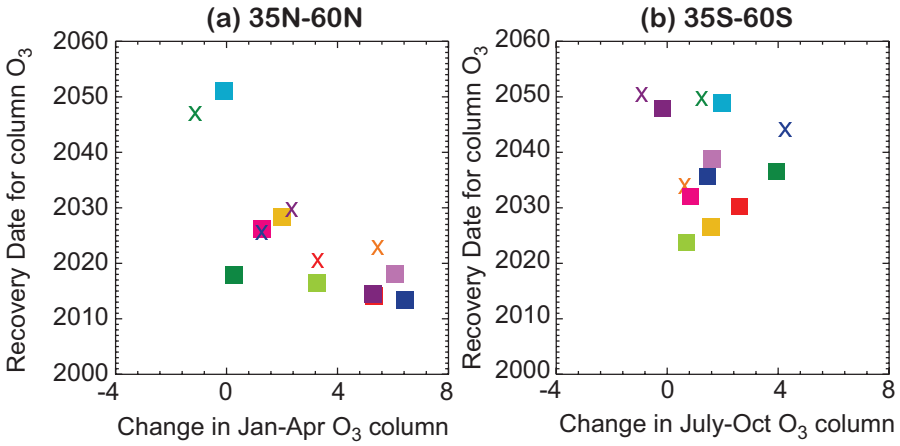

Figure 9.27: The relationship between the recovery date of mid-latitude (35°-60°) annual average ozone from the MMT analysis and the change in amplitude of the seasonal cycle of ozone averaged over the spring in each hemisphere. The change in the seasonal cycle is defined as the difference between 1960-1979 and 2040-2059 and is shown in panels (b) and (d) of Fig. 9.26. The averages are calculated for January-April and July-October for the NH and SH, respectively.

9.7 Summary

9.7.1 Summary by Model

Here, we provide a brief summary of the mean model ozone results. Summaries for each model are also provided, which identify differences from the multi-model mean, emphasizing where each model performs particularly well with respect to observations, or particularly poorly. For ozone recovery, comparisons are made with the multi-model mean.

Multi-model mean: In the tropics, the total ozone column for the multi-model mean agrees reasonably well with observations whereas in mid-latitudes, models are generally biased high by 10-20 DU. In the polar regions although the depth of the ozone hole is well reproduced in the multi-model mean, there is a wide spread in results and most models simulate an ozone hole that is too small in area. Arctic ozone in the multi-model mean is close to that observed, but there is a wide spread in results due to interannual variability in the polar vortex. The recovery properties of the multi-model mean have been discussed at length in Section 9.6.

AMTRAC3 has one of the smallest ozone depletions for the upper stratosphere due to low Cl_y. In the column amount, the model is only slightly lower than observed in the tropics and mid-latitudes, but has one of the largest losses in mid-latitudes. The model simulates the ozone hole reasonably well, but in the Arctic, the model column ozone is biased low. Ozone recovery is consistent with the multi-model mean in the SH, but tends to be late in the NH. AMTRAC3 O_3 is much more sensitive to NOy change in the tropics than most models.

CAM3.5 has a large high bias in ozone in the tropical upper stratosphere and one of the smallest depletions. In the column amount, the model is only slightly lower than observed in the tropics and mid-latitudes, but has one of the smallest depletions for the lower stratosphere and column ozone. This is likely due to the model Cl_y, which is one of the smallest. Polar ozone is biased high and the ozone hole is much smaller than observed due to a combination of high ozone bias and small area of PSCs (Chapter 4). Ozone recovery is consistent with the multi-model mean.

CCSRNIES has one of the largest cooling rates in the upper stratosphere, leading to a faster ozone recovery. The model has a high bias in the cold areas in the Antarctic late winter and spring, but the ozone hole is under-predicted in size and depth.

CMAM has a column ozone which is lower than observed in the tropics and northern mid-latitudes. The model has one of the largest tropical vertical ascent rates and corresponding change in lower stratospheric tropical ozone. The model has generally less ozone reduction than the multi-model mean, due to lower Cl_y levels. Ozone recovery in northern mid-latitudes is similar to the multi-model mean, but is early in the Arctic and in southern mid-latitudes. The simulated Antarctic ozone hole agrees reasonably well with observations, and the return to 1980 levels occurs at a similar year as the multi-model mean.

CNRM-ACM has a larger tropical and mid-latitude ozone reduction than observations due to chlorine and a corre-

sponding larger recovery than most models. The ozone change is particularly notable in the SH. In polar regions, past ozone loss and Cl_y are similar to that observed (Chapter 5). The Antarctic ozone hole, using a 220 DU theshold, is large in area, because of a low bias in the lower atmosphere.

EMAC has a small and shallow ozone hole, due in part to the region of low temperatures (T < 195 K) being smaller than observed.

E39CA has a high bias in ozone in the tropical upper stratosphere. In the column amount, the model has a high bias at all latitudes with the largest bias of all models in the tropics. The model has a small ozone hole area, based on a 220 DU threshold, due to an overall ozone bias. For both ozone and Cl_y, E39CA generally has the earliest recovery dates, which are roughly one decade prior to those of the multi-model mean.

GEOSCCM is similar to observations in the tropics, but the total ozone column is higher than observed in middle and high latitudes. Cl_y is similar to the multi-model mean but reduces faster in the future. The ozone hole is smaller and more shallow than observed because of the ozone bias. The model has one of the earliest returns to 1980 polar ozone values.

LMDZrepro has the deepest ozone hole of CCMVal-2, which give rise to the steepest gradients in ozone column at the edge of the southern polar vortex. However, the ozone depletion due to chlorine is at the low end of the model range and the model cooling rate is the largest in the upper stratosphere.

MRI is biased high at all latitudes compared with measurements of the total column ozone. The model has a large ozone column reduction due to chlorine increase, which is larger than most models. The model has a corresponding slower ozone recovery in the NH, but is near the model average for the SH. The depth of the ozone hole agrees well with observations, but the area of the ozone hole is much smaller than observed primarily because of the ozone high bias.

NiwaSOCOL is the same as SOCOL with a difference in the model lower boundary. Results are similar to SOCOL — no significant differences in the ozone hole diagnostics were seen.

SOCOL agrees with observations and the multi-model mean for tropical ozone for the first part of the simulation, but after about 2050, column ozone decreases substantially due to the large change in the BD circulation (Chapter 4). The circulation change gives rise to a strong cooling in the tropical lower stratosphere and a reduction of ozone. The model has a large reduction in Cl_y during the 21st century compared with the model mean, leading to a faster recovery. The simulated Antarctic ozone hole is in good agreement with observations for the current atmosphere, although low column ozone values are simulated early in the REF-B1 simulation due to dynamical influences.

ULAQ has an ozone column that is higher than observed for the past due to low Cl_y. The model ozone return to 1980 levels is near the multi-model mean in mid- and high latitudes of the NH, but is later than the mean in southern polar regions. After about 2040 ozone recovers faster than in most models. The simulated Antarctic ozone hole agrees reasonably well with observations, although low column ozone values are also simulated early in the REF-B1 simulation.

UMETRAC did not supply data in time to be evaluated.

UMSLIMCAT has an ozone column in all latitudes that is biased low, possibly because of a low bias in tropospheric ozone. Ozone recovers faster than in most models, particularly in the SH, due in part to Cl_y values being lower than the multi-model mean. The simulated Antarctic ozone hole is in reasonable agreement with observations.

UMUKCA-METO generally agrees with observations of the tropical and mid-latitude mean column ozone. In the tropical upper stratosphere, the model ozone change is similar to the multi-model mean, but the model is biased low due to very high chlorine. In southern mid-latitudes, the ozone column reduces unexpectedly after 2070. In the Arctic the simulated ozone column is reasonably consistent with observations, but in the Antarctic the model is biased high. The Antarctic ozone hole is small and shallow due to insufficient PSCs.

UMUKCA-UCAM is higher than observed for the total column ozone at all latitudes and is lower than most models in the upper stratosphere, due to higher Cl_y. Ozone recovery to 1980 levels is similar to the multi-model mean in the NH, and southern mid-latitudes, but is late over Antarctica. Due to a combination of the ozone bias, and low PSCs, the Antarctic ozone hole is small and shallow.

WACCM simulates a tropical total column ozone which is lower than observed. Tropical upper stratospheric ozone is higher than most models. In mid-latitudes and polar regions, the model agrees reasonably well with observation of the total column ozone. Column ozone recovers to 1980 values at about the same time as the multi-model mean in the SH, but earlier than the mean in the NH. The Antarctic

ozone hole is well simulated by the model, but disappears faster than in other models which simulate the ozone hole well.

9.7.2 Overall Summary

In this Chapter we have introduced a time series additive model (TSAM) analysis to make individual- and multi-model trend estimates, which may be used to make formal inference. One of the primary goals of this analysis was to produce more quantitative multi-model ozone projections with associated uncertainty estimates. Another goal was the careful comparison of ozone projections between the CCMVal-1 and CCMVal-2 data sets to identify areas where models have improved and areas that continue to require modelling effort. In the application of the TSAM analysis it is clear that a number of practical issues can influence this comparison (*e.g.*, longer, more complete time series of the period of interest were submitted to CCMVal-2 compared to CCMVal-1). Our findings are summarized below.

Most of the conclusions of the last WMO assessment remain unchanged. Ozone recovery time scales are very similar to those previously deduced, and several models in particular have undergone several major changes that have tended to reduce the overall spread of results. This provides more confidence in model trends. One important change from WMO (2007) is that some models now indicate that a small, residual ozone hole may still be present from 2060 until 2100 or later.

The results from CCMVal-2 have been analysed over broad latitudinal ranges. In the tropics, ozone does not change substantially in the simulations, and transport *i.e.*, upward motion is likely to be the largest driver. As a result, ozone decreases in the past, and recovers slightly due to chlorine decreases. In the second half of the 21st century, column ozone is expected to reduce once more, primarily due to the transport effect dominating chlorine reduction, which is essentially complete.

In mid-latitudes, chlorine and bromine are likely playing the most important role and consequently the narrower spread in simulated halogen amounts has led to a reduced spread in ozone simulations. In addition ozone transport is important in northern mid-latitudes.

In the Arctic ozone is very variable and difficult to simulate, due at least in part to the chaotic nature of dynamical processes. In addition there is no clear consensus on the trends in downwelling, and hence the amount of ozone transport is not clear compared with other impacts. In some cases models do not simulate well the Antarctic ozone hole, even when some allowance is made for the vortex edge or for the PSC areas, at least as defined in Chapter 4 by temperature threshold. No significant progress has been made on this since CCMVal-1 by most models. The large differences between the models could be due to differences in model chemistry. Another possibility is that the cloud microphysics may be being treated inadequately by some models (Chapter 6). For example if particle fall rates are too large during June and July, there would be no material surfaces in the warmer spring period for PSCs to form. While this would suggest that estimates of the date of disappearance of the ozone hole are unreliable, there is some consistency in the group of models which reproduce best the current ozone hole. These models suggest that a small, residual ozone hole will still be present from 2060 until the end of the simulations in 2100.

There is a need for a range of simulations looking at all aspects of the atmosphere-ocean system to try to address some of these issues. Uncertainties in net temperature changes, which arise from uncertainties in the increase of the strength of the BD circulation *versus* radiative changes, need to be reduced. Realistic bromine amounts need to be included in model simulations to allow for the short lifetime species known to be present (WMO, 2007, Chapter 2). Finally, simulations with fixed halogens or fixed GHGs need to be completed to complement the realistic simulations that have been completed to establish more rigorously the impact of climate and chemistry changes.

References

Austin, J. and F. Li, 2006. On the relationship between the strength of the Brewer-Dobson circulation and the age of stratospheric air, *Geophys. Res. Lett.*, **33**, doi:10.1029/2006GL026867.

Austin, J. and T. J. Reichler, 2008. Long term evolution of the cold point tropical tropopause: Simulation results and attribution analysis, *J. Geophys. Res.*, **113**, doi:10.1029/ 2007JD009768.

Austin, J. and R. J. Wilson, 2006. Ensemble simulations of the decline and recovery of stratospheric ozone, *J. Geophys. Res.*, **111**, doi:10.1029/2005JD006907.

Austin, J., K. Toupali, E. Rozanov, H. Akiyoshi, S. Bekki, G. Bodeker, C. Brühl, N. Butchart, M. Chipperfield, M. Deushi, V. I. Fomichev, M. A. Giorgetta, L. Gray, K. Kodera, F. Lott, E. Manzini, D. Marsh, K. Matthes, T. Nagashima, K. Shibata, R. S. Stolarski, H. Struthers, and W. Tian, 2008. Coupled chemistry climate model simulations of the solar cycle in ozone and temperature, *J. Geophys. Res.*, **113**, doi:10.1029/2007JD009391.

Bodeker, G. E., H. A. Struthers, and B. J. Connor, 2002. Dynamical containment of Antarctic ozone depletion, *Geophys. Res. Lett.*, **29**, doi:10.1029/2001GL014206.

Bodeker, G. E., H. Shiona, and H. Eskes, 2005. Indicators of Antarctic ozone depletion, *Atmos. Chem. Phys.*, **5**, 2603-2615.

Butchart, N., and A. A. Scaife, 2001. Removal of chlorofluorocarbons by increased mass exchange between the stratosphere and troposphere in a changing climate, *Nature*, **410**, 799-802.

N. Butchart, A. A. Scaife, M. Bourqui, J. de Grandpré, S. H. E. Hare, J. Kettleborough, U. Langematz, E. Manzini, F. Sassi, K. Shibata, D. Shindell and M. Sigmond, 2006. Simulations of anthropogenic change in the strength of the Brewer-Dobson circulation. *Clim. Dyn.*, **27**, 727-741.

Charlton-Perez, A., L. M. Polvani, J. Austin, and F. Li, 2008. The frequency and dynamics of stratospheric sudden warmings in the 21st century, *J. Geophys. Res.*, **113**, doi:10.1029/2007JD009571.

Daniel, J. S., S. Solomon, R. W. Portmann, and R. R. Garcia, 1999. Stratospheric ozone destruction: The importance of bromine relative to chlorine, *J. Geophys. Res.*, **104**, 23,871-23,880.

Deckert, R. and M. Dameris, 2008. Higher tropical SSTs strengthen the tropical upwelling via deep convection, *Geophys. Res. Lett.*, **35**, doi: 10.1029/2008GL033719.

Douglass, A. R., R. S. Stolarski, M. R. Schoeberl, C. H. Jackman, M. Gupta, P. A. Newman, J. E. Nielsen, E. L. Fleming, 2008. Relationship of loss, mean age of air and the distribution of CFCs to stratospheric circulation and implications for atmospheric lifetimes, *J. Geophys. Res.*, **113**, doi: 10.1029/2007JD09575.

Engel, A., T. Mobius, H. Bonisch, U. Schmidt, R. Heinz, I. Levin, E. Atlas, S. Aoki, T. Nakazawa, S. Sugawara, F. Moore, D. Hurst, J. Elkins, S. Schauer, A. Andrews, and K. Boering, 2009. Age of stratospheric air unchanged within uncertainties over the past 30 years, *Nature Geosci.*, **2**, 28-31.

Eyring, V., N. Butchart, D. W. Waugh, H. Akiyoshi, J. Austin, S. Bekki, G. E. Bodeker, B. A. Boville, C. Brhl, M. P. Chippereld, E. Cordero, M. Dameris, M. Deushi, V. E. Fioletov, S. M. Frith, R. R. Garcia, A. Gettelman, M. A. Giorgetta, V. Grewe, L. Jourdain, D. E. Kinnison, E. Mancini, E. Manzini, M. Marchand, D. R. Marsh, T. Nagashima, P. A. Newman, J. E. Nielsen, S. Pawson, G. Pitari, D. A. Plummer, E. Rozanov, M. Schraner, T. G. Shepherd, K. Shibata, R. S. Stolaarski, H. Struthers, W. Tian, and M. Yoshiki, 2006. Assessment of temperature, trace species, and ozone in chemistry-climate model simulations of the recent past, *J. Geophys. Res.*, **111**, doi:10.1029/2006JD007327.

Eyring, V., D. W. Waugh, G. E. Bodecker, E. Cordero, H. Akiyoshi, J. Austin, S. R. Beagley, B. A. Boville, P. Braesicke, C. Brhl, N. Butchart, M. P. Chippereld, M. Dameris, R. Deckert, M. Deushi, S. M. Frith, R. R. Garcia, A. Gettelman, M. A. Giorgetta, D. E. Kinnison, E. Mancini, E. Manzini, D. R. Marsh, S. Matthes, T. Nagashima, P. A. Newman, J. E. Nielsen, S. Pawson, G. Pitari, D. A. Plummer, E. Rozanov, M. Schraner, J. F. Scinocca, K. Semeniuk, T. G. Shepherd, K. Shibata, B. Steil, R. S. Stolaarski, W. Tian, and M. Yoshiki, 2007. Multi-model projections of ozone recovery in the 21st century, *J. Geophys. Res.*, **112**, doi:10.1029/2006JD008332.

Fioletov, V. E., G. E. Bodeker, A. J. Miller, R. D. McPeters, and R. Stolarski, 2002. Global ozone and zonal total ozone variations estimated from ground-based and satellite measurements: 1964-2000, *J. Geophys. Res.*, **107**, doi:10.1029/2001JD001350.

Fioletov, V. E. and T. G. Shepherd, 2003. Seasonal persistence of midlatitude total ozone anomalies, *Geophys. Res. Lett.*, **30**, doi:10.1029/2002GL016739.

Fomichev, V. I., A. I. Jonsson, J. de Grandpre, S. R. Beagley, C. McLandress, K. Semeniuk and T. G. Shepherd, 2007. Response of the middle atmosphere to CO2 doubling: Results from the Canadian Middle Atmosphere Model, *J. Clim.*, **20**, 1121-1144.

Forster, P. M., G. Bodeker, R. Schoeld, S. Solomon, and D. Thompson, 2007. Effects of ozone cooling in the tropical lower stratosphere and upper troposphere, *Geophys. Res. Lett.*, **34**, doi:10.1029/2007GL081994.

Fusco, A. C. and M. L. Salby, 1999. Interannual variations of total ozone and their relationship to variations of planetary wave activity, *J. Clim.*, **12**, 1619-1629.

Garcia, R. R., D. R. Marsh, D. E. Kinnison, B. A. Boville, and F. Sassi, 2007. Simulation of secular trends in the middle atmosphere, 1950-2003, *J. Geophys. Res.*, **112**, doi:10.1029/2006JD007485.

Garcia, R. R. and W. J. Randel, 2008. Acceleration of the Brewer-Dobson circulation due to increases in greenhouse gases, *J. Atmos. Sci.*, **65**, 2731-2739.

Garnkel, C. I. and D. L. Hartmann, 2007. Effects of El

Nino-Southern Oscillation and the Quasi-Biennial Oscillation on polar temperatures inthe stratosphere, *J. Geophys. Res.*, **112**, doi:10.1029/2007JD008481.

Gettelman, A., T. Birner, V. Eyring, H. Akiyoshi, S. Bekki, C. Bruhl, M. Dameris, D. E. Kinnison, F. Lefevre, F. Lott, E. Mancini, G. Pitari, D. A. Plummer, E. Rozanov, A. Stenke, H. Struthers, and W. Tian, 2009. The tropical tropopause layer, 1960-2100, *Atmos. Chem. Phys.*, **9**, 1621-1637.

Hitchcock, P., T. G. Shepherd, and C. McLandress, 2009. Past and future conditions for polar stratospheric cloud formation simulated by the Canadian Middle Atmosphere Model, *Atmos. Chem. Phys.*, **9**, 483-495.

Holton, J. R., and H.-C. Tan, 1980. The influence of the equatorial quasi-biennial oscillation on the global circulation at 50mb. *J. Atmos. Sci.*, **37**, 2200-2208.

Huck, P. E., S. Tilmes, G. E. Bodeker, W. J. Randel, A. J. McDonald, and H. Nakajima, 2007. An improved measure of ozone depletion in the Antarctic stratosphere, *J. Geophys. Res.*, **112**, doi: 11110.11029/12006JD007860.

Li, F., J. Austin, and J. Wilson, 2008. The strength of the Brewer-Dobson circulation in a changing climate: coupled chemistry-climate model simulations, *J. Clim.*, **23**, 40-57.

Li, F., R. S. Stolarski, and P. A. Newman, 2009. Stratospheric ozone in the post-CFC era, *Atmos. Chem. Phys.*, **9**, 2207-2213.

McLandress, C. and T. G. Shepherd, 2009a. Simulated anthropogenic changes in the Brewer-Dobson circulation, including its extension to high latitudes, *J. Clim.*, **22**, 1516-1540.

McLandress, C. and T. G. Shepherd, 2009b. Impact of climate change on stratospheric sudden warmings as simulated by the Canadian Middle Atmosphere Model, *J. Clim.*, **22**, 5449-5463.

Manzini, E., M.A. Giorgetta, M. Esch, L. Kornbluh, and E. Roeckner, 2006. The influence of sea surface temperatures on the northern winter stratosphere: Ensemble simulations with the MAECHAM5 model, *J. Clim.*, **19**, 3863-3881.

Miller, A. J., R. M. Nagatani, L. E. Flynn, S. Kondragunta, E. Beach, R. Stolarski, R. D. McPeters, P. K. Bhartia, M. T. DeLand, C. H. Jackman, D. J. Wuebbles, K. O. Patten, R. P. Cebula, 2002. A cohesive total ozone data set from SBUV(/2) satellite system, *J. Geophys. Res.*, **107**, doi:10.1029/2001JD000853.

Newman, P. A., J. S. Daniel, D. W. Waugh, and E. R. Nash, 2007. A new formulation of equivalent effective stratospheric chlorine (EESC), *Atmos. Chem. Phys.*, **7**, 4537-4552.

Oman, L., D. W. Waugh, S. Pawson, R. S. Stolarski, and P. A. Newman, 2009. On the influence of anthropogenic forcings on changes in the stratospheric mean age, *J. Geophys. Res.*, **114**, doi:10.1029/2009JD010378.

Oman, L., D. W. Waugh, S. R. Kawa, R. S. Stolarski, A. R. Douglass, and P. A. Newman, 2010. Mechanisms and feedbacks causing changes in upper stratospheric ozone in the 21st century, *J. Geophys. Res.*, **115**, doi:10.1029/2009JD012397, In press.

Portmann R. W., and S. Solomon, 2007. Indirect radiative forcing of the ozone layer during the 21st century, *Geophys. Res. Lett.*, **34**, doi:10.1029/2006GL028252.

Pawson, S., R. S. Stolarski, A. R. Douglass, P. A. Newman, J. E. Nielsen, S. M. Frith, and M. L. Gupta, 2008. Goddard Earth Observing System chemistry-climate model simulations of stratospheric ozone-temperature coupling between 1950 and 2005, *J. Geophys. Res.*, **113**, doi:10.1029/2007JD009511.

Plumb, R.A., 1996. A "tropical" pipe model of stratospheric transport, *J. Geophys. Res.*, **101**, 3957-3972.

Randel, W. J. and F. Wu, 2007. A stratospheric ozone prole data set for 1979-2005: Variability, trends and comparisons with column ozone data, *J. Geophys. Res.*, **112**, doi:10.1029/2006JD007339.

Shepherd, T. G., 2008. Dynamics, stratospheric ozone and climate change, *Atmos.-Ocean*, **46**, 117-138.

Shine, K. P., M. S. Bourqui, P. M. de F. Forster, S. H. E. Hare, U. Langematz, P. Braesicke, V. Grewe, M. Ponater, C. Schnadt, C. A. Smith, J. D. Haigh, J. Austin, N. Butchart, D. T. Shindell, W. J. Randel, T. Nagashima, R. W. Portmann, S. Solomon, D. J. Seidel, J. Lanzante, S. Klein, V. Ramaswamy, and M. D. Schwarzkopf, 2003. A comparison of model-simulated trends in stratospheric temperatures, *Quart. J. Roy. Meteorol. Soc.*, **129**, 1565-1588.

Son, S.-W., L. M. Polvani, D. W. Waugh.,T. Birner, H. Akiyoshi, R.R. Garcia, A. Gettelman, D. A. Plummer and E. Rozanov, 2008. The impact of stratospheric ozone recovery on tropopause height, *J. Clim.*, **22**, 429-445.

Stolarski, R. S., and S. Frith, 2006. Search for evidence of

trend slowdown in the long-term TOMS/SBUV total ozone data record: The importance of instrument drift uncertainty, *Atmos. Chem. Phys.*, **6**, 4057-4065.

Struthers H., G. E. Bodeker, J. Austin, S. Bekki, I. Cionni, M. Dameris, M.A. Giorgetta, V. Grewe, F. Lefevre, F. Lott, E. Manzini, T. Peter, E. Rozanov, and M. Schraner, 2009. The simulation of the Antarctic ozone hole by chemistry-climate models, *Atmos. Chem. Phys.*, **9**, 6363-6376.

Takahashi, M., 1996. Simulation of the stratospheric quasi-biennial oscillation using a general circulation model, *Geophys. Res. Lett.*, **23**, 661-664.

Tie, X., and G. Brasseur, 1995. The response of stratospheric ozone to volcanic eruptions: Sensitivity to atmospheric chlorine loading, *Geophys. Res. Lett.*, **22**, 3035-3038.

Tilmes, S., D. E. Kinnison, R. R. Garcia, R. Müller, F. Sassi, D. R. Marsh, and B. A. Boville, 2007. Evaluation of heterogeneous processes in the polar lower stratosphere in the Whole Atmosphere Community Climate Model, *J. Geophys. Res.*, **112**, doi:10.1029/2006JD008334.

Waugh, D. W., 2009. The age of stratospheric air, *Nature Geosci.*, **2**, 14-16.

Waugh, D. W., L. Oman, S. R. Kawa, R. S. Stolarski, S. Pawson, A. R. Douglass, P. A. Newman, and J. E. Nielsen, 2009. Impact of climate change on stratospheric ozone recovery, *Geophys. Res. Lett.*, **36**, doi:10.1029/2008GL036223.

World Meteorological Organization (WMO)/United Nations Environment Programme (UNEP), 2007. *Scientific Assessment of Ozone Depletion: 2006*, World Meteorological Organization, Global Ozone Research and Monitoring Project, Report No. 50, Geneva, Switzerland.

Yang, Q., Q. Fu, J. Austin, A. Gettelman, F. Li, H. Vömel, 2008. Observationally Derived and GCM Simulated Tropical Stratospheric Upward Mass Fluxes, *J. Geophys. Res.*, **113**, 2008JD009945.